Experimental determination of the water demand for urban green spaces

J. Bertrand

Delft University of Technology

TU Delft

Experimental determination of the water demand for urban green spaces

by

J. Bertrand

Thesis committee:	J. A. van der Werf, supervisor
	E. Andrusenko
	A. M. J. Coenders
	J. G. Langeveld
Project Duration:	September, 2025 - May, 2026
Faculty:	Faculty of Civil Engineering and Geosciences, Department of Environmental Egineering

TU Delft

Abstract

Cities are increasingly implementing urban green spaces to cope with the challenges of climate change, including more intense droughts and heat stress. Urban green spaces currently rely largely on drinking water for irrigation, often at rates exceeding the actual water demand of the vegetation. Better understanding of this water demand could help improve irrigation efficiency and reduce pressure on drinking water availability. This study investigates whether the minimal water demand of urban green spaces can be determined experimentally. A mass balance approach is applied to MeSUDa (Managed experimental Sustainable Urban Drainage Area), an isolated vegetated bioswale located at the Flood Proof Holland site on the TU Delft campus. The setup consists of three compartments with different drainage configurations. By measuring precipitation, outgoing drainage, and changes in soil water storage, evapotranspiration is determined as the rest term of the water balance. The observation period ran from 17 October 2025 to 19 January 2026. Only one of the compartments could be used to apply the mass balance method to. The cumulative precipitation over the observation period was 350.6 mm, though this carries uncertainty due to a 34% discrepancy with data from the official KNMI station at Rotterdam The Hague Airport. The cumulative outgoing drainage was 51.8 mm. The storage change component could not be fully quantified for the entire soil profile. The soil moisture sensors, installed at 10 and 25 cm depth, only represent the upper 0.35 m of the approximately 1.15 m deep profile. Attempts to further constrain the storage change using a nighttime water balance analysis, an event-based rainfall threshold method, a graphical approach, and time lag analysis between soil moisture sensors did not produce results sufficient to close the water balance. The cumulative water balance could not be closed due to an incomplete quantification of the storage change over the full soil profile, possible overestimation of precipitation, or a combination of both. The conclusion of this thesis is that, within the current setup and observation period, it was not possible to experimentally determine the minimal water demand of urban green spaces. The mass balance approach applied to MeSUDa is in principle well suited for this purpose, but reliable determination of all water balance components is a necessary condition.

Contents

Abstract i

Nomenclature iii

1 Introduction 1

2 Methodology 4
2.1 The mass balance approach . . . 4
2.2 The Experimental Setup: MeSUDa . . . 5
2.2.1 Physical lay out of MeSUDa . . . 6
2.2.2 Materials and soil properties & Vegetation . . . 6
2.2.3 Instrumentation and Measurement in MeSUDa . . . 9
2.3 Scope of the water balance approach . . . 12
2.3.1 Reference magnitudes of the water balance components . . . 12
2.4 Experimental Determination of Mass Balance Components . . . 14
2.4.1 Area and weather conditions during observed period . . . 14
2.4.2 Precipitation and Irrigation . . . 15
2.4.3 Water depth with respect to the bottom of the compartment . . . 15
2.4.4 Outgoing drainage . . . 15
2.4.5 Storage change . . . 16
2.5 Water balance over the entire observation period . . . 22

3 Results and Discussion 23
3.1 Sensor data quality check . . . 23
3.1.1 Statement about snow processes and frozen soil conditions . . . 29
3.2 Results of the mass balance components . . . 29
3.2.1 Precipitation component . . . 30
3.2.2 Outgoing drainage component . . . 30
3.2.3 Storage change components . . . 31
3.3 Results water balance over the entire observation period . . . 39

4 Conclusions 41

5 Recommendations 43
5.1 Further verification of precipitation data . . . 43
5.2 Outgoing drainage component validation . . . 43
5.3 Quantifying storage change over the whole soil profile . . . 43
5.4 Change of observation period and observation length . . . 44

References 45

A Figures 49
A.1 Figures and Images chapter . . . 50

Nomenclature

Abbreviations

Abbreviation	Definition
BGI	Blue-Green Infrastructure
DTW	Dynamic Time Warping
EC	Eddy Covariance
ET	Evapotranspiration
FAO	Food and Agriculture Organization
FPH	Flood Proof Holland
GIS	Geographic Information System
KNMI	*Koninklijk Nederlands Meteorologisch Instituut* (Royal Netherlands Meteorological Institute)
LDPE	Low Density Polyethylene
MeSUDa	Managed experimental Sustainable Urban Drainage Area
NetCDF	Network Common Data Form
vwc	volumetric water content

Symbols

Symbol	Definition	Unit
CF	Correction factor for tipping bucket area to compartment area	[-]
D	Outgoing drainage	[mm/h]
$D_{cumulative}$	Cumulative outgoing drainage	[mm]
ET	Evapotranspiration	[mm/h]
$ET_{cumulative}$	Cumulative evapotranspiration	[mm]
ET_{ref}	Makkink reference evapotranspiration	[mm]

Symbol	Definition	Unit
$I_{after,prune}$	Lower bound estimate of water storage on vegetation and first 10 cm of soil after pruning	[mm]
$I_{before,prune}$	Lower bound estimate of water storage on vegetation and first 10 cm of soil before pruning	[mm]
I_{plants}	Lower bound estimate of interception reservoir of the plants	[mm]
I_{soil}	Lower bound estimate of water stored in the first 10 cm of soil	[mm]
Ir	Irrigation input	[mm/h]
k_{sat}	Saturated hydraulic conductivity	[m/s]
P	Precipitation	[mm/h]
P_{air}	Air pressure	[Pa]
$P_{cumulative}$	Cumulative precipitation	[mm]
P_{diver}	Pressure measured by diver	[Pa]
P_{night}	Cumulative nighttime precipitation	[mm]
$P_{watercolumn}$	Hydrostatic pressure of water column above diver	[Pa]
S	Water storage per unit area	[mm]
S_{end}	Upper layer storage value at end of night	[mm]
S_{start}	Upper layer storage value at start of night	[mm]
z	Vertical depth coordinate	[m]
ΔS_{night}	Upper layer storage difference over the night	[mm]
$\Delta\theta_{response}$	Soil moisture response to rainfall event	[m³/m³]
θ	Soil moisture level	[m³/m³]
$\theta(z)$	Soil moisture profile as function of depth	[m³/m³]
θ_{10}	Soil moisture level at 10 cm depth	[m³/m³]
θ_{25}	Soil moisture level at 25 cm depth	[m³/m³]
θ_{post}	Maximum soil moisture during response window	[m³/m³]
θ_{pre}	Antecedent soil moisture before rainfall event	[m³/m³]

1

Introduction

Cities are implementing Blue-Green Infrastructure (BGI) to make urban environments more resilient to the challenges of climate change [1]. Blue-green infrastructure (BGI) combines the use of vegetation (green) and water features (blue) to create a synergistic effect that enhances passive urban cooling [2]. Under this definition also fall urban green spaces, which are semi-natural systems such as bioswales, green roofs, and street trees. These systems are are designed to provide ecological, hydrological, and social benefits within cities [3], [4]. Urban green spaces, as a key component of BGI, have useful properties under which to manage storm water [5]. Urban green spaces can temporarily hold storm water on-site, reducing the volume and rate of water entering the sewer system [6]. Peak flow reductions of up to 70–80% have been reported in some BGI studies [7], directly relieving the load on the conventional sewer infrastructure during storm events. Next to temporary storage, BGI elements reduce total runoff volume by allowing water to infiltrate to the soil or taken up and transpired by the plants so that it does not reach the sewer at all [8]. Another benefit of BGI is that it reduces urban heat primarily by shading and evaporative cooling [9], [10], [11]. Shading refers to the interception of short-wave solar radiation by vegetation canopy, which reduces heat absorption, heat storage, and the emission of long-wave radiation from shaded built surfaces, while providing substantial reduction of mean radiant temperatures [12]. Evaporative cooling results from evapotranspiration (ET) which involves not only the transfer of water from plants to the atmosphere, but also from soil to atmosphere [12]. All these benefits together make urban green spaces an option for cities to cope with increasing temperatures and more intense precipitation events.

However, climate change will also increase extreme precipitation events as well as the temperature and the severity and duration of droughts in the summer in the future [13], [14]. Therefore, at some point in time the precipitation will not be enough to maintain urban green spaces. Currently, urban green spaces are largely maintained using drinking water for irrigation [15]. This puts additional stress on the availability of drinking water and therefore the production of drinking water. In turn, this will make circumstances for people in the cities more intense [16], as drinking water availability is already under pressure during drought periods. Studies show that the water use for irrigation is higher than the demand of the vegetation [17], [18], [19]. [17] directly compared measured irrigation consumption across 110 large parks and 1882 small parks in the metropolitan area of Santiago, Chile, with modeled vegetation water requirements. They found that the water use for irrigation was higher than the modeled vegetation demand, indicating a potential to save water. Over-irrigation was found to be a widespread practice, primarily caused by extensive lawn surfaces and ornamental plants with high water requirements. Public green spaces were found to be considerably more water efficient than private residential gardens, because they were applying excessive watering to avoid any appearance of water stress in the vegetation. [18] looked at the impact of 14 commonly used BGI types on household water balance under climate projections in the Netherlands and highlighted the importance of the difference between current irrigation norms and actual urban vegetation needs. Applying agricultural and forestry irrigation standards to urban green spaces can lead to overuse of water resources, as these guidelines are designed for crop growth stages and maximizing yield. In urban green spaces, especially during

drought, the priority is to sustain plant life using a minimal amount of water. [19] analyzed the irrigation efficiency of six parks in Beijing across dry, moderate, and wet years, finding that in most parks precipitation alone already exceeded evapotranspiration (which represents the actual water demand of the vegetation) but the irrigation was still applied at rates as high as 581.95 mm/m². Even in parks where a real water deficit existed, the applied irrigation was 2.24 to 7.95 times higher than the deficit, showing over-irrigation in urban green spaces. The overuse of irrigation for urban green spaces calls for the need of better irrigation management. Additionally, municipalities responsible for maintaining urban green spaces often operate under limited budgets. By better understanding and managing the demand for these green spaces, financial resources can be used more efficiently, potentially freeing up money for improved monitoring of urban water systems as well as the implementation of more efficient irrigation strategies or systems [20], [21].

By understanding the water demand of urban green spaces, irrigation can be managed more efficiently, helping to reduce the overuse of water and putting less pressure on the drinking water stock. Existing approaches to estimate the water demand of vegetation, such as the FAO Penman-Monteith method, rely on reference evapotranspiration calculations combined with crop coefficients [22], [23]. These methods are well established, they are derived largely from agricultural settings and may not accurately represent the water demand of the mixed, low-maintenance vegetation types that are typically used in urban green spaces [24]. When improving irrigation efficiency in urban green spaces, the focus should shift from potential evapotranspiration towards the minimum water demand required to maintain plant survival and health. In addition, the estimation of evapotranspiration and subsequently plant water requirements in urban vegetation needs to consider the heterogeneity of plants, soils, water, and climate characteristics [25]. [26] applied an eddy covariance method to directly measure ET in the urban environment of Berlin, Germany. The eddy covariance technique measures turbulent fluxes of latent and sensible heat at a flux tower, but frequently produces data gaps of up to 60% annually due to instrument failures and low turbulent atmospheric conditions. To account for these gaps, flux footprint modeling was combined with machine learning techniques to gap-fill and model ET at a half-hourly resolution. The methods also used remote sensing and GIS data to account for the spatial heterogeneity of urban land cover. Although this approach achieved an R^2 of 0.84 at a vegetated site, it requires extensive instrumentation and expertise, limiting its applicability to small-scale urban green spaces. Also, a challenge of the eddy covariance method in urban environments is that the surface area affecting the flux measurements, the flux footprint is not fixed. It changes continuously depending on wind speed, wind direction, and atmospheric stability. An experimental approach, in which the actual water fluxes of an urban green space are directly measured under real outdoor conditions, could provide a more site-specific and reliable estimate for the water demand of urban green spaces.

Therefore, the research question of this thesis project is therefore: ”Is it possible to determine the minimal water demand of urban green spaces experimentally?”

To answer this question, a mass balance approach is applied to an experimental setup called MeSUDa (Managed experimental Sustainable Urban Drainage Area), an isolated vegetated bioswale located at the Flood Proof Holland site on the TU Delft campus. By measuring precipitation, outgoing drainage, and changes in soil water storage, evapotranspiration is determined as the rest term of the water balance. The experimental setup is divided into 3 section or compartments. This division allows for controlled experimentation, with one compartment serving as a control and the other two as experimental compartments. The hydrological conditions of the compartments can also be varied, in order to test for different hydrological conditions. The MeSUDa setup is isolated from the soil where it is founded on so it is designed to take away the influx of water from the surrounding soil. Because transpiration is typically the dominant component of evapotranspiration in vegetated systems, this provides a direct measure of the water demand of the vegetation [22]. The observation period runs from 17 October 2025 to 19 January 2026.

A similar experimental approach and setup was applied by [27], which used a mass balance method to directly measure water fluxes of vegetation under real outdoor conditions using a weighing lysimeter. However, their setup did not allow for the simultaneous comparison of different hydrological conditions within a single experiment. MeSUDa addresses this by partitioning the setup into three isolated compartments with different drainage configurations, multiple hydrological conditions. Next to that, MeSUDas vegetation consist of plants that are commonly applied in practice in typical swales and Blue-Green

Infrastructure by landscape architects. While their are other researches that are using a mass balance approach to estimate the water demand of the vegetation [15], MeSUDa is small scale and isolated from water influxes of the surrounding soil by the way it is constructed.

The report is structured as follows: chapter 2 describes the mass balance approach with its scope and the MeSUDa study area with its physical layout instrumentation. This chapter also discusses methods on how to determine the precipitation component, the outgoing drainage component and the storage change component of the water balance. This chapter also provides reference values for the water balance components. Eventually it describes a method for a check of the cumulative magnitudes for the water balance components. Chapter 3 describes a sensor data quality check to confirm the usability of the data from the instrumentation. After that the results of the methods to determine each water balance component are presented and discussed. Eventually the cumulative water balance is applied to the determined components to verify the correctness of the cumulative magnitudes of the water balance components. Chapter 3 is followed by chapter 4 and 5 that contain the conclusion and the recommendations of this thesis respectively.

2

Methodology

This chapter describes the mass balance approach and how it is used to obtain the water demand of urban green spaces. It also provides an overview of the experimental setup where the mass balance approach is applied to. After that the scope of the water balance is outlined and reference values for the water balance components are established. Next, methods on how to determine each water balance component are described. The last section provides the water balance over the entire period which serves as a check, to check if the water balance components have been determined correctly.

2.1. The mass balance approach

To address the main research question, whether the water demand of urban green spaces can be determined experimentally, this study makes use of a mass balance approach, applied to an experimental setup called MeSUDa. The details about the MeSUDa setup will be discussed in section 2.2. But in short MeSUDa is an isolated vegetated bio-swale system, where the bio-swale consist of 3 layers (also see figure 2.1).
A mass balance approach identifies the dominant hydrological fluxes within a defined volume. On a given time interval, the change in water storage within this control volume is determined by incoming and outgoing water fluxes. Incoming fluxes consist of precipitation and irrigation, when applied. The outgoing fluxes are the drainage from the system and the evapotranspiration. By quantifying precipitation, drainage, and changes in soil water storage, evapotranspiration can be determined as the rest term of the water balance according to equation 2.1. The water balance and its main fluxes is also schematically depicted in figure 2.1. Because the walls of the MeSUDa setup are raised above the most upper soil layer, surface run off is not considered as a flux. When surface run off occurs, it stays with in the control volume and exits by evaporation or infiltration and then drainage.

$$ET(t) = P(t) + I_r(t) - D(t) - \frac{dS}{dt} \tag{2.1}$$

where:

- ET is the evapotranspiration in [mm/h],
- P is the in [mm/h],
- I_r is the irrigation input in [mm/h],
- D is the outgoing drainage in [mm/h], and
- $\frac{dS}{dt}$ is the rate of change of water storage in [mm/h].

Evapotranspiration represents the combined water loss due to soil evaporation and plant transpiration and interception evaporation [22], [18]. In vegetated systems such as MeSUDa, transpiration is typically the dominant component and is directly related to plant water uptake. So determining evapotranspiration provides a direct measure of the water demand of the vegetation in the system. This

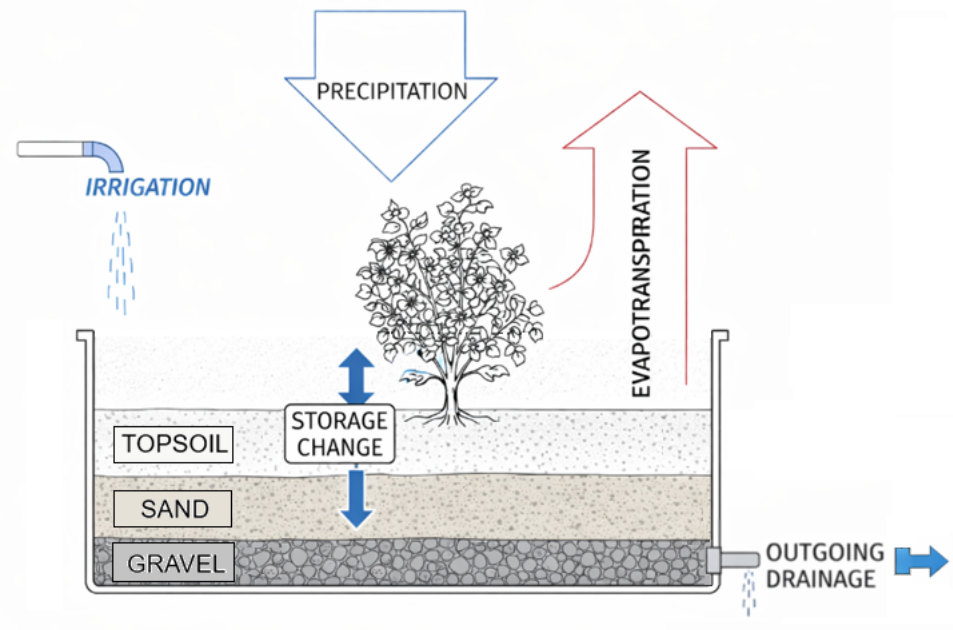

Figure 2.1: Schematic figure of the main fluxes of the hydrological fluxes of the mass balance

is under the assumption that plants are not water-stressed. Evapotranspiration reflects the amount of water required to maintain plant physiological processes and growth, making it a suitable approximation for the plant water demand [22], [28]. Therefore, the main objective of the mass balance approach is to estimate the water demand of the plants in the setup via the evapotranspiration. The next sections describe the experimental setup where the mass balance is applied on and reference values and behavior of water balance fluxes. It also outlines what is included within the scope of this thesis.

2.2. The Experimental Setup: MeSUDa

The experimental setup that is used in this study was constructed, among others, by former MSc student C.E. Martin in 2024/2025 [29]. In their thesis, Martin designed and constructed an open air lab, which was intended to “inform research, practice, and educational activities for eco-based sustainable water management,” with an emphasis on the enablement of long-term performance monitoring while still supporting short-term experiments [29], [30]. They called this open air lab MeSUDa, **M**anaged **e**xperimental **S**ustainable **U**rban **D**rainage **A**rea. MeSUDa will also be the experimental area for the current project. MeSUDa was designed as a bioswale with a gradual slope split into ”three sections to monitor long-term vegetated swale hydrological and bio-chemical behaviour”. MeSUDa is located at the Flood Proof Holland (FPH) site. This a site run by TU Delft’s Green Village and VP Delta for outdoor experiments and demonstrations. FPH is located on the southern end of the TU Delft campus [30].
In the next subsections the physical layout of MeSUDa, the materials and vegetation used in constructing the setup and the instrumentation that is present in MeSUDa is described.

2.2.1. Physical lay out of MeSUDa

(a) Bare MeSUDa foundation

(b) Base layer with a 2% slope

(c) Partitioning of MeSUDa into three compartments

(d) Front view of MeSUDa (October 2025)

Figure 2.2: Overview of MeSUDa structural layout [29]

Figure 2.2 gives a general overview of the main structural features of MeSUDa. Sub-figures 2.2a and 2.2b depict the concrete retaining walls that form the foundation of MeSUDa and the base layer that creates a 2 % slope, respectively. The light slope promotes drainage for each compartment. In sub-figure 2.2c, the partitioning into three different compartments of equal size is seen. The setup is partitioned with the use of wooden dividers and a LDPE plastic lining was used to isolate the compartments from each other. The lining was draped over the barriers and outer walls. In sub-figure 2.2d a front view of MeSUDa with vegetation.
An overview of the dimensions of the concrete foundation of MeSUDa can be found in figure A.1.

2.2.2. Materials and soil properties & Vegetation

With the physical layout established in the previous subsection, this subsection now presents the materials, soil properties and vegetation of MeSUDa.

Materials overview of MeSUDa

Figure 2.3 and table 2.1 provide an overview of all materials used to construct MeSUDa. The soil properties of the fill media of MeSUDa can be found in table 2.2. Like mentioned earlier, the concrete foundation of MeSUDa is divided into 3 compartments using wooden dividers (6). This division allows for controlled experimentation, with one compartment serving as a control and the other two as experimental compartments.
The impermeable LDPE plastic lining (7) is used to isolate the compartments from each other and from the base layer (1) to prevent leakage and interaction between compartments and possibly the ground soil. The lining was affixed to the barriers and walls and smoothed as much as possible, To prevent preferential flow paths.
On top of the plastic lining, underdrains (8) are installed at the bottom of each compartment. They consist of a perforated PVC pipe (8a) with filter stocking to prevent clogging. This perforated PVC pipe is connected to a non-perforated PVC pipe (8b), which is slid through the concrete plastic lining and concrete foundation to form an outlet drain for each compartment. An adhesive was used to seal the lining around each pipe to prevent leakage. MeSUDa features two different kind of outlet drains (9 & 10) as can be seen in sub figure 2.3b. Compartment A and B have a free-flowing outflow configuration

(9), while compartment C has an enforced water table configuration (10). This allows Compartment C to have different hydrological conditions than Compartments A and B.
The fill medium of MeSUDa consists of the sloped base layer (1) , and on top of that successive layers of: gravel and coarse sand (2) that cover the underdrains, fine sand (2) and the topsoil (4). There is a layer of wood chips (5) present in compartment C, this is because MeSUDa was originally designed to also study the effects of enhanced nitrate removal by addition of a supplementary organic carbon source. The tree planting soil was specifically chosen as topsoil for its lower infiltration capacity to promote a longer residence time, and therefore an extended treatment period, in MeSUDa [29], [30]. A drainage ditch (11) has been dug at the front of MeSUDa to drain the water from the outlets of the compartments to a channel nearby.

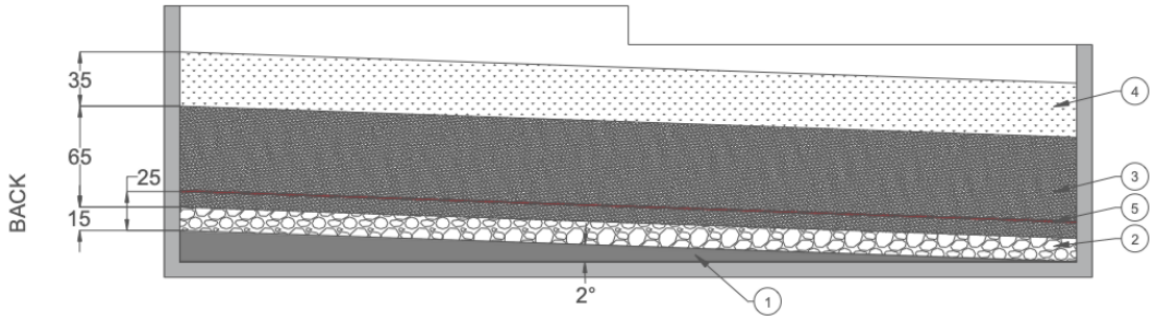

(a) Schematic side view of the soil layers (all dimensions in cm)

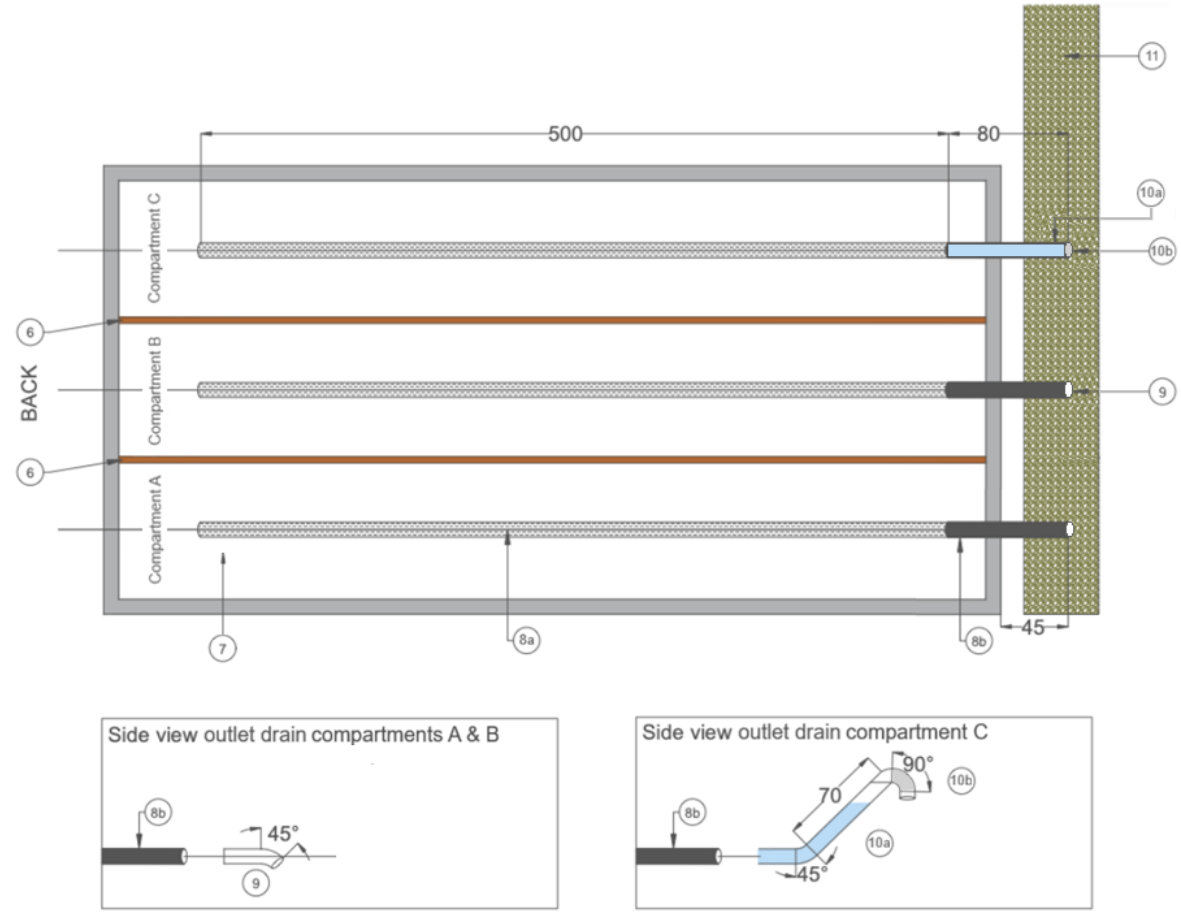

(b) Schematic top view of MeSUDa (all dimensions in cm)

Figure 2.3: Layers and materials of MeSUDa. This figure is linked to table 2.1 and adapted from [29]. All dimensions are in cm.

Table 2.1: Construction Materials and Specifications for MeSUDa [29].

Number in figure 2.3	Material Name	Specification	Description
1	base material	Heterogenous mixture of sand and rocky soil.	Available at FPH, used to construct 2% slope.
2	gravel + coarse sand	See table 2.2 for details.	Available at FPH.
3	fine sand	Classified as sandy loam. See table 2.2 for details.	Available at FPH.
4	topsoil	Tree planting soil (*bomengrond*). Classified as sandy clay loam. See table 2.2 for details.	Selected for low infiltration capacity (approx. 0.25 cm/h), as tested in [30].
5	woodchips	Installed in compartment C with thickness = 1 cm, depth = 90 cm.	Available at FPH. Calculated mass of approx. 16.5 kg. Assumed to be conifer species.
6	wooden divider	Wood planks, approx. 3 cm in thickness.	Available at FPH.
7	impermeable lining	LDPE 0.5 mm plastic sheeting.	Used to isolate each compartment and prevent leakage.
8	underdrain	$\varnothing_{\text{internal}}$ 50 mm PVC, total length = 5.8 m. 5 m perforated (8a) and 0.8 m non-perforated (8b).	Placed at the bottom of **each** swale to collect and drain water at outlets.
9	outlet drain, free-flowing	$\varnothing_{\text{internal}}$ 50 mm PVC joint with 45° bend.	Directs outflow downwards to drainage ditch (11).
10	outlet drain, enforced water level	$\varnothing_{\text{internal}}$ 50 mm PVC, 45° joint connected to 70 cm of straight pipe (10a) with 90° joint at end (10b).	Creates water table of 50 cm in the connected swale. Excess water is directed downwards.
11	drainage ditch	Dug-in ditch, width = 30 cm, depth = 25 cm.	Drains water from MeSUDa into nearby channel.

Table 2.2: Grain size analysis findings from [30].

	Topsoil	Fine sand	Gravel
Bulk density [g/m^3]	0.96	1.81	1.60
Porosity [-]	0.64	0.32	0.40
Organic matter [%]	7	0.13	0.20
Clay [%]	15	<0.1	<0.1
Silt [%]	10	<0.1	<0.1
k_{sat} [m/s]	1.4e-5	2e-3	>2

MeSUDa's vegetation composition

Plant species differ in their transpiration rates, leaf surface area, and root water holding and uptake capacities. Consequently, the evapotranspiration of MeSUDa is influenced by the plant species present. A picture from the vegetation of October 2025 is seen in figure 2.4. The plant species that are present in MeSUDa can be found in table 2.3. This selection of plants is made because they are commonly applied in practice in typical swales and Blue-Green Infrastructure by landscape architects. In practice, such vegetation is usually applied as pre-mixed flower/seed mixtures, developed for low-maintenance public spaces such as swales, road verges, and sidewalks. They were planted once and then evenly distributed across the three compartments, without a specific division per compartment.

Figure 2.4: Picture of vegetation growing in MeSUDa taken 17 October 2025

Table 2.3: Overview of the vegetation present in MeSUDa.

MeSUDa's vegetation		
1. Coreopsis	7. Calendula	13. Cornflower
2. Dill	8. Purple Coneflower	14. Sneezeweed
3. Zinnia	9. Cosmos	15. Ox-Eye Sunflower
4. Borage	10. Wallflower	16. Hyssop Lavender
5. Crimson Clover	11. Cosmos Sensation	17. Bergamot
6. Aster	12. Black-Eyed Susan	18. Prairie Clover

2.2.3. Instrumentation and Measurement in MeSUDa

The MeSUDa experimental setup also features instrumentation in order to detect certain hydrological fluxes and behavior within the three compartments, as well as materials to irrigate the compartments. An overview of these can be found in figure 2.6 and table 2.4.

Figure 2.5 gives pictures of the monitoring and data logging instruments of MeSUDa. Those instruments provide data in the form of time series. The N° notation is related to the location numbers in

table 2.4. The weather station (N°8), shown in figure 2.5a, provides information of the precipitation. The weather station is located at the Green Village on the TU Delft campus, which is roughly 1.5 km from the location of MeSUDa. Figure 2.5b shows one of the types of soil moisture sensors (N°1) used in MeSUDa. MeSUDa has two pairs of soil moisture sensors per compartment: one pair located at the front of the compartment and one at the back. The sensors are installed in the topsoil, positioned directly above one another at depths of 10 cm and 25 cm. They provide time series of the soi moisture of the soil at those points. Figure 2.5c shows a picture of one of the three tipping buckets (N°6). They are connected to the outlet drainage pipes of each compartment and provide a time series of the amount of water that flows out of the compartment. Finally, figure 2.5d gives a picture of a real-time water level monitor using a pressure sensor, a diver (N°2). These divers are used to check if there is a water table building up in the compartments.
The water reservoir (N°4), the water can (N°5) and the perforated tube (N°7) can be used to irrigate the compartments.

Now that the study area and experimental setup are outlined, the next section will discuss the methods of obtaining and quantifying the mass balance components.

(a) Davis Vantage Pro2 weather station [31]

(b) Example of a type of soil moisture sensor: Decagon 5TM watercontent sensor [32]

(c) ECRN-100 rain gauge

(d) Van Essen TD-Diver: water level datalogger [33]

Figure 2.5: Overview of monitoring and data-logging instruments in MeSUDa

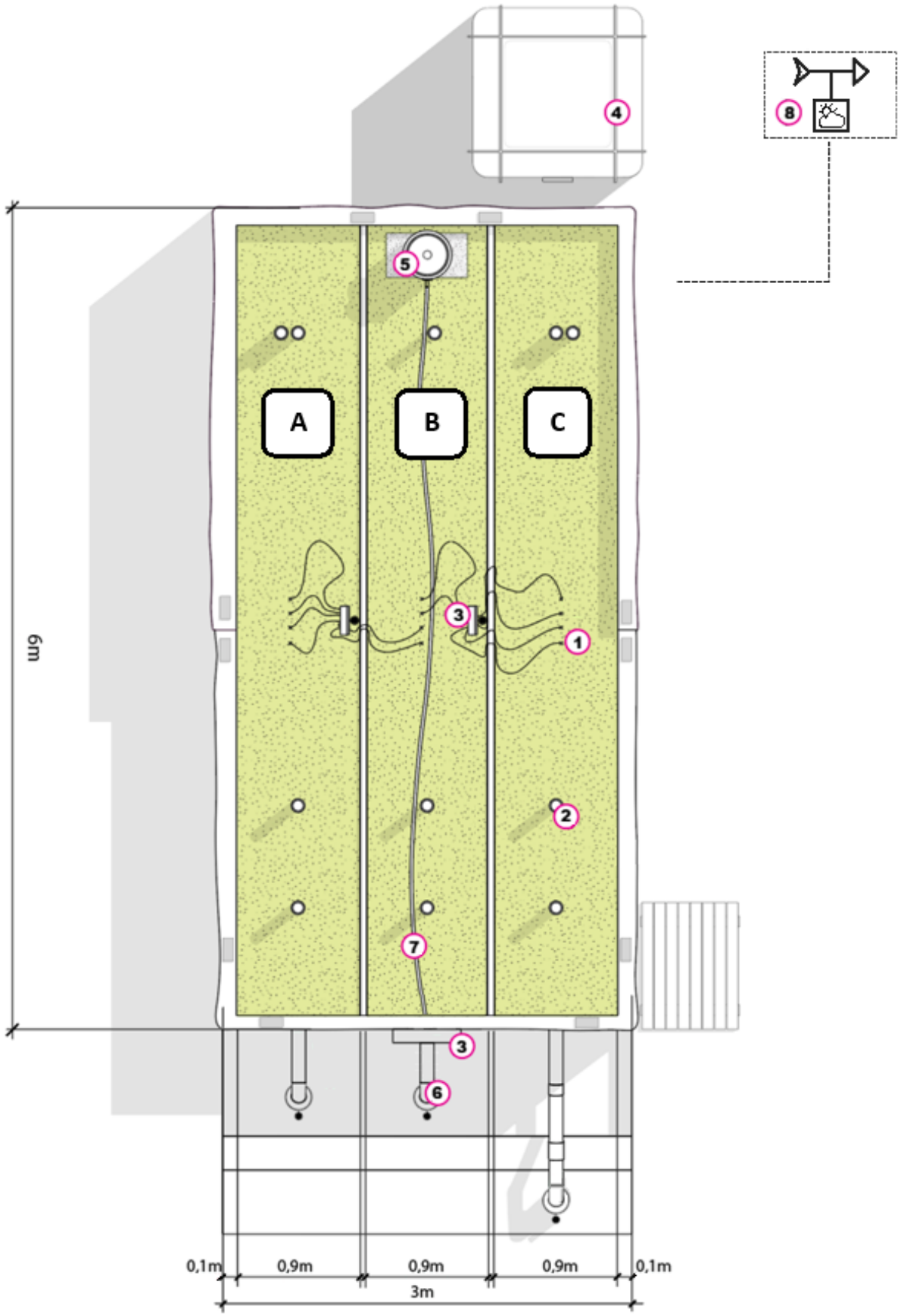

Figure 2.6: Schematic top view of MeSUDa with its instrumentation and irrigation material. The descriptions of the numbers can be found in table 2.4

Table 2.4: Overview of the instrumentation and irrigation material present in MeSUDa. N° are linked to figure 2.6

N°	Feature Name	Specification	Description
1	Soil moisture sensors	Soil moisture sensors (METER TEROS 12 (3), Decagon 5TM (8), Decagon ECHO EC-5 (1)	Provides soil moisture data at two depths (10 cm and 25 cm), with two sensors per depth profile (four per compartment, 1 pair in the front and 1 in the back). This helps to identify wilting point and to control the fixed water table compartment. And provides information of the speed of the wetting front
2	Divers	Van Essen TD-Divers (6) (2 per compartment) positioned 20 cm away from the walls	Creates data regarding water depth per compartment, helps to identify wilting point and control the fixed water table compartment
3	Data receivers	ZL6 data receiver (3)	Two receivers are connected to the soil moisture sensors, and one to the tipping buckets, allowing for phone log storage and image analysis
4	Water reservoir	1000 L (1.0 m × 1 m × 1 m) plastic container	Storage and holding unit for water, used for the forced water table section
5	Water can	60 L plastic container with a tube for forced irrigation	(Intermediate) holding unit, for distriution of water over the compartment via the perforated tube (N° 7)
6	Tipping buckets	ECRN-100 tipping buckets (3)	Used to quantify the amount of water that is draining from the compartments via their outlets
7	Perforated tube	A regular perforated tube that can run from the water can to the end of a compartment	The perforated tube is connected to the water can and is used to distribute the water from the water can for forced irrigation
8	Weather station	A Davis Vantage Pro2 weather station, located approximately 1.5 km from FPH site	Used to quantify precipitation

2.3. Scope of the water balance approach

The water balance as applied in this study considers precipitation and irrigation as the only incoming fluxes, and outgoing drainage and evapotranspiration as the only outgoing fluxes. Several processes that could in reality contribute to the water balance of MeSUDa are not considered. First, leakage through the LDPE lining is assumed to be negligible, as the lining was installed to isolate the compartments from each other and from the surrounding soil. However, imperfections in the lining, such as folds or gaps around the outlet drainage pipe connections, could introduce unquantified water losses that would be attributed to evapotranspiration in the rest term. Second, capillary rise from deeper soil layers below the gravel layer is assumed negligible, because of the concrete foundation base and of the impermeable lining at the base. When reading the thesis these simplifications need to be kept in mind while reading the method and the results.

2.3.1. Reference magnitudes of the water balance components

To be able to assess whether the measured fluxes are physically plausible and consistent with the expected hydrological behavior of MeSUDa, reference values for each component of the water balance must be established.

For precipitation, the data from the weather station at the Green Village on the TU Delft campus is used directly. To verify the reliability of these measurements, they are compared to precipitation recorded at the official KNMI weather station at Rotterdam The Hague Airport, which is the nearest official KNMI station to the FPH site.

The cumulative precipitation over the entire observation period according to the weather station at Rotterdam the Hague Airport is 260.2 mm. Figure 2.7 compares the precipitation values between the data from the Green Village and Rotterdam Airport. It is seen that the cumulative rainfall according to the Green Village data is 350.6 mm which is 34 % higher compared with the cumulative rainfall according to the data of Rotterdam Airport. This is a high difference. This questions the reliability of the precipitation data and therefore it should be interpreted with caution. The weather station at Rotterdam Airport is likely of higher quality and uses well-calibrated gauges. Nevertheless, the precipitation dataset from the Green Village weather station is used in this study. This choice is made because the Green Village location is approximately 1.5 km from the FPH site, whereas the Rotterdam Airport station is approximately 4.7 km away. Due to the spatial variability of precipitation, the station closest to the site is considered more representative and prioritized over measurement differences. The cumulative precipitation of Rotterdam Airport is 90 mm lower this introduces uncertainty in the analysis made in this study. The overall shape of the time series are similar, but during the October month Rotterdam Airport displays higher rainfall amounts and during the January month Green Village produces higher values.

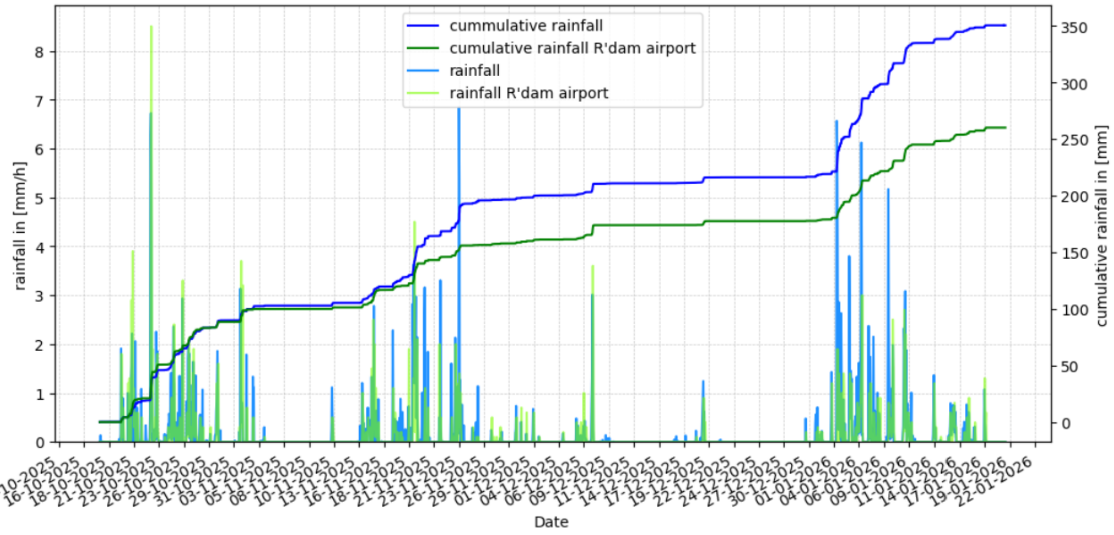

Figure 2.7: Rainfall amount and cumulative rainfall for the entire observation period for precipitation values according to weather stations at the Green Village TU Delft and at Rotterdam The Hague Airport. Time resolutions are both 1 hour.

For evapotranspiration, a reference value is obtained from the monthly Makkink reference evapotranspiration values published by KNMI for De Bilt. Makkink requires the incoming shortwave radiation and the mean daily temperature to calculate the reference evaporation for a particular day [34]. By summing the monthly Makkink ET values for October, November, December and January, a cumulative reference ET for the observation period can be obtained. This value provides an independent order-of-magnitude estimate against which cumulative evapotranspiration values can be compared.

An overview of the cumulative evapotranspiration according to the weather station at the Bilt can be found in table 2.5. According to this data, the total evapotranspiration over the observation period is 42.8 mm for the entire observation period.

Table 2.5: Table of the Makkink reference evaporation in mm of weather the Bilt of the entire observation period per month [35].

Month	$\mathbf{ET_{ref}}$ [mm]
17 - 31 October	11.0
November	13.8
December	8.1
1-19 January	9.9
Total: 42.8 mm	

For storage, the maximum possible water storage of a compartment is estimated from the physical dimensions and soil properties of the fill medium of MeSUDa. The total pore volume available for water storage in a compartment can be estimated as the product of the compartment volume and the porosity of each soil layer. The compartment dimensions and soil layer thicknesses as well as the porosity are known from the construction of MeSUDa as described in section 2.2.2.

The results of the pore volume estimation per soil layer per compartment of MeSUDa can be found in table 2.6. As seen in the table the total pore volume of one compartment is 2.55 m^3, which is 489 mm of water storage that is possible in one compartment. It is also seen in the table that the top layer has the largest pore volume of the three layers. The upper bound for the water storage in the upper layer of a compartment, according to table 2.6, is 1.16 m^3 /(0.9 · 5.8) m^2 = 222 mm. So 222 mm is the maximum possible storage in the upper 0.35 m of topsoil assuming all pores are filled with water, which means it represents the storage when the soil is fully saturated.

Table 2.6: Total pore volumes available for water storage per layer per compartment [30]

Layer	**Porosity** [-]	**Layer volume m^3**	**Layer pore volume m^3**
Top soil	0.64	1.82	1.16
Fine sand	0.32	3.39	1.08
Gravel	0.40	0.78	0.31
			Total = 2.55 m^3

For outgoing drainage, no independent reference value can be determined prior to the measurements. Instead, an estimated bound of the expected drainage is obtained from the water balance as D = P − ET, under the assumption that the net storage change over the observation period is negligible. If the net storage change is not negligible and storage increased over the observation period, the actual cumulative drainage will be lower than this bound, because part of the precipitation is retained in the soil rather than draining out. If storage decreased over the period, drainage could in principle exceed this value, because water from before the observation period could have also drained out.

The result of the bound that is obtained via the water balance and the cumulative precipitation and cumulative evaporation values can be seen in table 2.7.

Table 2.7: A bound for the cumulative drainage over the entire observation period, with ET the Makkink reference evapotranspiration and P the cumulative rainfall over the period

P [mm]	ET [mm]	**D [mm]**
350.6	42.8	**307.8**

This boundary value, D = 307.8 mm, is not a measured result, but an assumption-based estimate that can be interpreted as a reference or upper bound for drainage, depending on the storage change. The actual drainage depends on if the storage change increased or decreased over the entire observation period.

2.4. Experimental Determination of Mass Balance Components

This section discusses how the different components of the water balance, as described in equation 2.1 and in section 2.1, are determined. The individual hydrological fluxes are quantified using the instrumentation described in Section 2.2.3. The digital sensor data is processed using Jupyter Notebooks, which provide an accessible and transparent workflow. The following subsections present an overview of the methods used to preprocess the sensor data, examine them and prepare them as usable inputs for the mass balance equation.

2.4.1. Area and weather conditions during observed period

The documented observation period was from 17-10-25 until 19-01-26. During these months, the weather conditions and the MeSUDa setup changed. Changes that need to be noted in weather condi-

tions are that during the observed months the evapotranspiration is much lower compared to the summer months [35], due to the lower incoming shortwave radiation [34]. These low evaporation months are suitable for closing the water balance because it is then easier to identify leakages, storage losses and measurement errors. Also, during the observation period the plants in the MeSUDa setup were pruned on 30-11-2025 for every compartment, see figure 2.8. This decreased the water interception ability of the plants. Lastly, in the period 3-12 January, the weather conditions were cold with days below the freezing point and heavy snowfall on the 3rd,5th,7th and 9th of January.

(a) before **(b)** after

Figure 2.8: Pictures of MeSUDa before and after pruning the plants. Pruning date 30-11-25

2.4.2. Precipitation and Irrigation

The precipitation is measured by the weather station present at the Green Village on the TU Delft campus, which is located roughly 1.5 km from the location of MeSUDa. The precipitation time series are retrieved from NetCDF files obtained from the Ruisdael Data Platform [36]. The data are provided at a temporal resolution of 1 minute and expressed in units of mm h^{-1}. The time series can be converted to alternative temporal resolutions by resampling the data to the target resolution using mean or sum aggregation over fixed time intervals. In addition, the data can be converted to precipitation amounts and cumulative precipitation. These processing steps enable the analysis of precipitation at different values and temporal resolutions.

Intentional irrigation could be performed with the water can and the perforated tube (number 5 and 7 respectively of figure 2.6). But during the observation, no irrigation was applied. Precipitation is the only input to the water balance model during this thesis. After pre-processing, the precipitation data from the weather station can directly be used as component of the water balance.

2.4.3. Water depth with respect to the bottom of the compartment

Inside each compartment there are two divers installed, one in the front and one in the back of the compartment. These divers are placed in vertically positioned perforated pipes that reach up into the gravel layer. They measure the hydrostatic pressure of the water column above the sensor if there is any present. So, they obtain data on the water depth in the compartments and therefore if there is water level in the compartment.

Because the divers measure pressure and not depth with respect to the bottom of the compartments, their values have to be corrected. To account for the air pressure that also contributes to the pressure measured by the divers, the air pressure has to be subtracted from the diver pressure value in order to obtain the hydrostatic pressure of the water column above the diver. The correction looks like $P_{watercolumn} = P_{diver} - P_{air}$. The diver data will mainly be used to check whether there is a water level build up inside the compartments

2.4.4. Outgoing drainage

Tipping buckets are connected to the outlet drains of each compartment and they are rain gauges that measure the outflow of the compartment. They collect the water from the outlet drains through a

funnel and direct it to a double-bucket mechanism. This mechanism collects the water in one of its two buckets, and when the bucket is full, the mechanism tips to one side. As a result, the bucket is emptied and a signal is send to the sensor; each tipping event is recorded, hence the name tipping bucket. See figure 2.9.

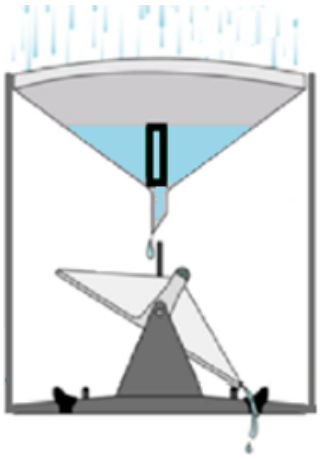

Figure 2.9: Schematic crossection of a tipping bucket rain gauge [37]

The ECRN-100 tipping buckets that are used in MeSUDa have a volume of 4.02 ml/tip and rain depth of 0.2 mm per tip listed in the specifications [38]. So the surface where the tipping bucket calculates its values over is A_{bucket} = $4.02 \cdot 10^{-6}$ m^3 / 0.0002 m = 0.0201 m^2. The surface area of the compartment is $A_{compartment}$ = 0.9 · 5.8 m^2. So to correct the tipping bucket values that the data logger provides to the area of compartment, they are multiplied with a correction factor of CF = A_{bucket} / $A_{compartment}$ = (0.0201/0.9·5.8).

Due to the design of the tipping bucket, it is prone to errors. These errors can come from mechanical movement against the housing of the tipping bucket, which may cause the bucket mechanism to tip without there being any actual outflow. This unintended movement can be from accidental contact of humans or movement caused during the resealing of the lids. Additionally, water that accumulates in the ditch below the tipping buckets can, when the water level becomes sufficiently high, enter the tipping bucket through the drainage openings in the housing. This may also result in tipping events without corresponding outflow. Lastly, there is also the possibility that the lids of the tipping buckets are not fully sealed. Water may accumulate on the lids and leak through the space between the lid and the outlet pipe of the compartment, causing tips

To account for these errors, a filter threshold is applied to the tipping bucket data in order to remove outliers. The threshold is determined empirically using the drainage data of compartment C. Since the outlet drain of compartment C is configured such that drainage should only occur when the water level exceeds 50 cm, and this water level was never reached during the observation period, any recorded drainage in compartment C can then be attributed to these errors. The maximum outgoing drainage recorded in compartment C at a 1 hour resolution is 0.458 mm over the compartment area. A value of 0.46 mm is therefore used as the filter threshold for the outgoing drainage of the compartments. The time series can also be resampled using sum aggregation over fixed time intervals just like the precipitation data. After pre-processing, conversion to the right area and error filtering, the outgoing drainage can be directly used as component for the mass balance.

2.4.5. Storage change

The compartments of MeSUDa all contain two pairs of soil moisture sensors. They are placed directly above each other at two different depths, with one pair in the front and one pair in the back of the compartment. The soil moisture sensors were installed in the upper soil layer (see figure 2.3a) to monitor moisture conditions within the active root zone. Placing them there allows for detection of soil moisture levels approaching the permanent wilting point, and therefore providing information about potential plant water stress. In addition, changes in soil water storage due to soil evaporation can be detected,

because evaporation primarily occurs near the soil surface. Since the plants of the herbaceous and shallow-rooted species that are used in MeSUDa are concentrated in the upper soil layer, this zone is also where most water uptake for transpiration takes place. This makes it a relevant depth for monitoring soil moisture changes related to evapotranspiration.

The sensors provide the soil moisture levels) of the soil in m^3/m^3. The soil moisture is defined as the volume of water per the total volume of soil [39]. The soil moisture values are in a 5 minute time resolution and can also be resampled to different target resolutions when needed, also using mean aggregation over fixed time intervals. The soil moisture sensors were calibrated using field measurements under three reference conditions: dry (0 m^3/m^3), wet (0.375 m^3/m^3), and saturated water (1 m^3/m^3). For each individual sensor, a linear relationship between the measured sensor output and the corresponding reference value was fitted ($y = ax+b$). The derived calibration coefficients were then applied to all raw time series data to obtain calibrated soil moisture levels for further analysis. Unlike the other mass balance components, the storage change is not directly measured by any instrumentation. The soil moisture sensors measure the soil moisture at four locations per compartment and only within the upper soil layer. Alternative approaches must be undertaken to determine the storage change component.

Upper layer storage estimation

The approach below describes a method for determining the storage change in the upper 0.35 m of soil. This can be used to partially quantify the storage change component of the water balance for the whole soil profile. This approach was implemented by using the soil moisture measurements of the soil moisture sensors at the two different depths. Figure 2.10 displays a schematic front view of a compartment, here the location of the the soil moisture sensors can be seen. The method reconstructs a continuous vertical soil moisture profile from these point measurements and integrates it over depth to estimate total water storage.

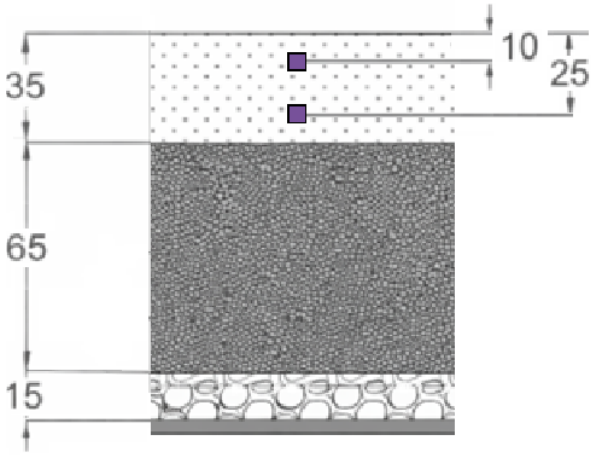

Figure 2.10: Schematic front view of a compartment of MeSUDa with the location of the soil moisture sensors depicted in purple (all dimensions in cm).

The symbol for soil moisture that is used is θ. Let θ_{10}(t) be the soil moisture level measured at 0.10 m depth and θ_{25}(t) at 0.25 m depth. A linear variation of soil moisture with depth is assumed between the two sensor locations. The change of soil moisture with vertical depth is therefore calculated according to equation 2.2

$$\frac{d\theta}{dz} = \frac{\theta_{25} - \theta_{10}}{0.25 - 0.10} \tag{2.2}$$

With this assumption, the soil moisture profile θ(z) at time t can be expressed as seen in equation 2.3. This is a one-dimensional (1D) vertical soil profile. This means that soil water dynamics are considered to vary only as a function of depth z, while changes in the horizontal directions are neglected. In other words, the control 'volume' is assumed to represent a vertically oriented soil column with uniform

hydraulic conditions across its horizontal extent. This means that water flow occurs only vertically and horizontal changes in soil moisture are neglected.

$$\theta(z) = \theta_{10} + \frac{d\theta}{dz}(z - 0.10) \tag{2.3}$$

Because measurements were only available between 0.10 m and 0.25 m, the linear trend was extrapolated to the upper and lower boundaries of the considered upper soil layer, so to z= 0 m and to z = 0.35 m. Now that the soil moisture profile θ(z) is known, the storage per unit area can be calculated by taking the integral of θ(z), see equation 2.4. The resulting storage S(t) represents the equivalent water depth in meters stored within the upper 0.35 m soil profile.

$$S(t) = \int_0^{0.35} \theta(z)\, dz \tag{2.4}$$

Because two independent pairs of soil moisture sensors were installed, one pair can be used as a control to check and compare the storage estimates derived from the other pair. The result is data, continuous in time, of storage in the upper layer derived from discrete depth measurements.

Night time water balance analysis

The method for evaluating the water balance during the night times with the use of the upper layer storage change as described by equation 2.4 is presented here. If the cumulative rainfall and drainage during the night correspond to the observed upper layer storage change, it indicates that the measured fluxes describe the system well. During the night, evapotranspiration can be assumed negligible, which simplifies the water balance. This makes it possible to check whether the remaining components close the balance.
This nighttime water balance provides an independent consistency check of the precipitation and outgoing drainage component with the upper layer storage change component. This is done to see if the upper layer storage change component is representative for the whole soil profile.

Nighttime intervals were defined as the time between sunset and the subsequent sunrise. Using these periods allows the water balance to be simplified, as evapotranspiration can be assumed to be approximately zero. Therefore the night time water balance becomes equation 2.5, where P_{night} is the cumulative precipitation over the night, D_{night} the cumulative outgoing drainage over the night and ΔS_{night} the upper layer storage difference over the nights .

$$P_{night} - D_{night} = \Delta S_{night} \tag{2.5}$$

For each nighttime interval, the upper layer storage at the beginning and end of the night is determined from the previously calculated upper layer storage time series. Because the storage data is recorded at discrete time intervals, the storage values closest in time to the night start and night end are selected. The nighttime change in upper layer storage is then calculated as: $\Delta S_{night} = S_{end} - S_{start}$. With S_{end} the upper layer storage value at the end of the night and S_{start} the upper layer storage at the beginning of the night. For each identified nighttime period, the cumulative rainfall and cumulative drainage are calculated. This is done by summing all rainfall and drainage measurements that occur between the start and end of the night. The soil moisture dynamics are also analyzed for the night periods. For both the upper and lower sensor, the soil moisture value at the start and end of the night is determined, and the total change over the nighttime period is calculated. This allows the short-term dynamics of soil moisture during the night to be examined when necessary.

Estimation of time lag between the two soil moisture sensors

The following part describes two methods of estimating the time lag between the two soil moisture sensors. The first method uses cross-correlation between the values of the two different soil moisture sensors to see at what time lag the correlation value is maximized. The second method used is dynamic time warping (DTW), to obtain a time-dependent estimate of the lag between the upper and lower soil moisture responses.

The time lag between soil moisture sensors provides information about how fast the water moves between the two soil moisture sensors in the top soil layer. If this travel time is known an estimation can be made for when it arrives at the bottom of the upper layer and moves into the sand layer. Knowing this, it could help estimate how much water leaves the topsoil, thereby constraining the storage change in the deeper part of the profile. This can help further quantifying the storage change for the whole soil profile.

Cross-correlation is a statistical technique that measures the similarity between two time series as a function of a time shift between them [40].Because the soil moisture sensors are located directly underneath each other, the upper sensor reacts earlier than the lower one and therefore there is a time lag between the two soil moisture sensor signals.
First the changes in soil moisture are calculated by taking the difference between consecutive measurements. Then the mean is removed from both time series to ensure that the correlation only looks at the temporal changes around the average behavior [41], [42]. The cross-correlation function is then computed for a range of positive and negative time lags. This function quantifies how well the changes in the upper and lower soil moisture sensors correspond when one signal is shifted relative to the other. A positive lag indicates that the lower sensor responds after the upper sensor, which can be interpreted as the time required for the moisture signal to propagate through the soil profile. The cross-correlation function can then be evaluated for a range of time lags. The lag corresponding to the maximum correlation value is interpreted as the statistical best estimate of the time lag between the responses of the two soil moisture sensors.

Dynamic time warping (DTW) is an algorithm for measuring the similarity between two temporal sequences which may vary in speed [43]. This approach is particularly useful when similar patterns occur in both time series but with varying timing or response rates [44]. Before applying the algorithm, the soil moisture time series are normalized to remove differences in magnitude between the sensors.
The DTW algorithm then determines the optimal alignment between the upper and lower soil moisture time series by minimizing the distance between the two signals. The result of the algorithm is a warping path that describes how the two time series would be aligned in time. From this alignment, the difference between the matched indices of the two signals is extracted. When it is then multiplied with the time resolution of the two soil moisture signals, the difference in indices is converted to the time lag between the sensors in minutes. After this, the time evolution of the lag can be analyzed and related to factors such as rainfall events.

Quantifying lower bound estimate of water storage on vegetation and first 10 cm of soil

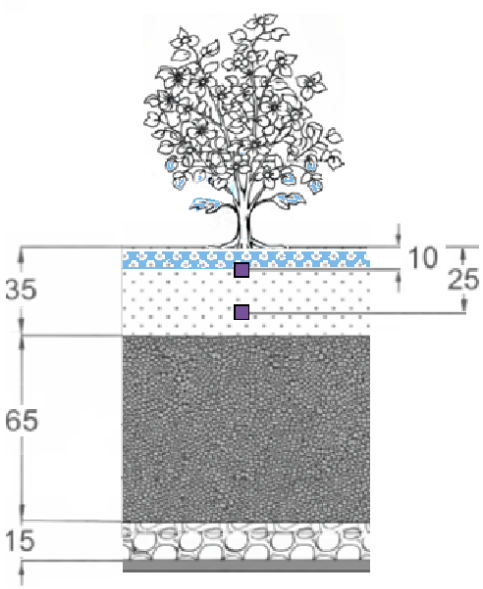

Figure 2.11: Schematic front view image of the soil profile and the vegetation of MeSUDa. The purple squares indicate the location of the soil moisture sensors and all dimensions are in cm.

In the method described in this section, an attempt is made in quantifying a lower bound for the amount of rainfall that can be temporarily stored on plant surfaces or in the upper 10 cm of soil (see figure 2.11). This storage occurs before the water infiltrates further into the soil profile or before drainage occurs. The estimation of this lower bound is done by combining precipitation measurements with soil moisture observations at 10 cm depth and drainage measurements.

The goal of this analysis is to isolate the amount of water stored on the plants and thereby further quantify the storage change component. This is because, in the upper-layer storage change, the water stored on the vegetation is not accounted for, since this storage change is based only on data from the soil moisture sensors.

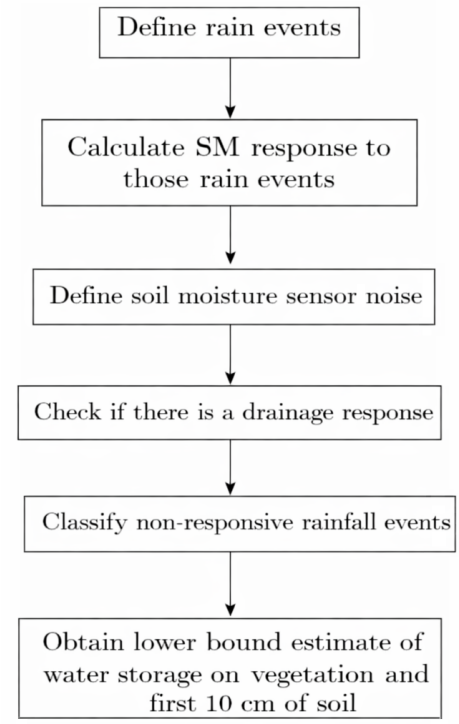

Figure 2.12: Steps of the rainfall threshold event-based analysis for quantifying water storage on vegetation and first 10 cm of soil

Figure 2.12 gives an overview of the steps of this method described in this section. The first step is the identification of what is considered to be an individual rainfall events. Rainfall events are defined as continuous periods during which precipitation is recorded (P > 0). Each time step where rainfall occurs after a dry time step marks the beginning of a new rainfall event. For each event, the start time, end time, duration, and total rainfall depth is determined. Events with very small rainfall totals are removed using a minimum rainfall threshold. This is to exclude negligible precipitation that is unlikely to produce a hydrological response.

To determine whether rainfall infiltrates into the soil profile, the response of the soil moisture sensors is evaluated for each rainfall event. The soil moisture response is quantified by comparing the antecedent soil moisture to the post-event soil moisture. Antecedent soil moisture is defined as the mean soil moisture during a time window preceding the start of the rainfall event. After the rainfall event ends, a response window is defined in which the maximum soil moisture value is determined. Separate response windows are used for the two sensors to account for differences in infiltration timing between depths. The soil moisture response at each depth is then calculated as seen in equation 2.6

$$\Delta\theta_{response} = \theta_{post} - \theta_{pre} \tag{2.6}$$

Where θ_{pre} is the antecedent soil moisture and θ_{post} is the maximum soil moisture level during the previously defined response window. The maximum level is used because it results in the most conservative

response by ensuring that not all smaller soil moisture levels are classified as responses.

Because soil moisture sensors exhibit measurement noise, small fluctuations in soil moisture may occur even when no real hydrological change takes place. To account for this, the magnitude of sensor noise is estimated using dry nighttime periods. Dry nights are defined as consecutive nights in a period with zero rainfall. The change in soil moisture between consecutive measurements is assumed to represent measurement noise. These consecutive nights are the nights of dry period 04-11-25 till 09-11-25. The 99th percentile and not the 95th percentile of the absolute soil moisture changes is used as a conservative estimate of the sensor noise threshold for each sensor depth. The sensor noise is determined separately and noise is assumed constant over time.

In addition to soil moisture changes, drainage measurements are analyzed to detect whether rainfall water is leaving the compartment. For each rainfall event, the drainage volume is summed over a specified period following the event. The drainage response window is limited to either a fixed duration after the event or the start of the next rainfall event, whichever occurs first. This prevents drainage from a subsequent rainfall event from being incorrectly attributed to the previous event.

In addition to soil moisture changes, drainage measurements were evaluated following each rainfall event to determine whether measurable outflow occurred during the following period. The drainage response window was limited to either a fixed duration after the event or the start of the next rainfall event, whichever occurs first. This approach does not attempt to attribute drainage to individual rainfall events, but rather tries to be as a conservative filter to exclude events where water left the system after rainfall.

Using the precipitation, soil moisture, and drainage responses, rainfall events are classified according to whether they produce a self- defined detectable hydrological response. A rainfall event is considered an non- responsive rainfall event when the following conditions are satisfied:

- the soil moisture increase at 10 cm does not exceed the sensor noise threshold
- no measurable drainage occurs following the event

Events that meet these criteria are interpreted as rainfall events for which all incoming water is temporarily stored on the plants surface or in the first 10 cm of topsoil. The capacity of the water stored on vegetation and first 10 cm of soil is then estimated as the maximum rainfall depth among all non-responsive rainfall events. This value represents the largest rainfall event that can take place without producing a soil moisture response in the upper sensor or measurable drainage. This value is then interpreted as a conservative lower-bound estimate of the water storage on vegetation and first 10 cm of soil of the compartment.

Like stated in section 2.4.1, the plants in all the compartments were pruned at 30-11-25. This provides data with plants and data without plants. Before the pruning the water storage that is being investigated in this section consists of the interception on the plant and the water in the first 10 cm of soil. Lets call this, $I_{before,prune} = I_{plants} + I_{soil}$. After the pruning the the water storage that is being investigated in this section, only consists of the water stored in the first 10 cm of soil, so $I_{after,prune} = I_{soil}$. With this information the lower bound of the the water storage on the vegetation and first 10 cm of soil, can be estimated separately according to equations 2.7 and 2.8 respectively.

$$I_{plants} = I_{before,prune} - I_{after,prune} \tag{2.7}$$

$$I_{soil} = I_{after,prune} \tag{2.8}$$

Where:

- $I_{before,prune}$ is the lower bound estimate water storage on the vegetation and first 10 cm of soil, before the pruning moment and
- $I_{after,prune}$ the lower bound estimate of the water storage on the vegetation and first 10 cm of soil, after the pruning moment and
- I_{plants} the lower bound estimate of the interception reservoir of the plants of MeSUDa and

- I_{soil} the lower bound estimate of the water stored in the first 10 cm of soil.

A visual aid for interpreting equations 2.7 and 2.8 is provided in figure 2.13.

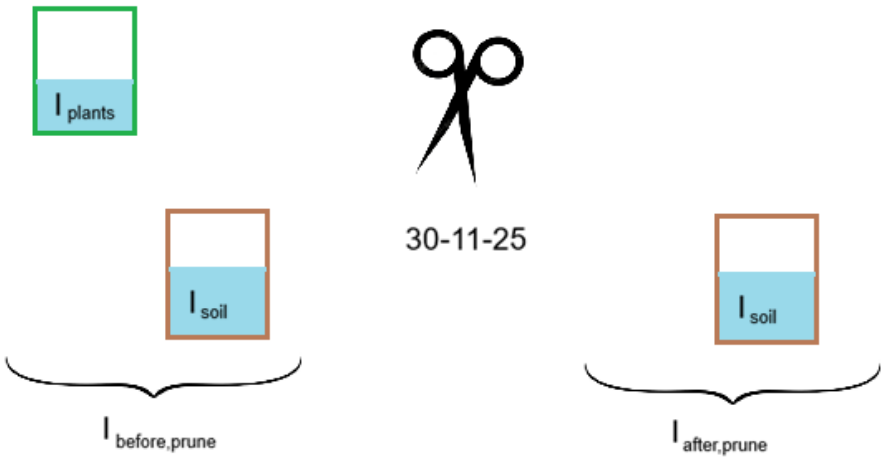

Figure 2.13: Schematic supporting figure intended to aid interpretation of equations 2.7 and 2.8

Graphical approach

An additional graphical approach was applied to estimate the lower bound of the water storage on the vegetation and first 10 cm of soil. For this approach, a dry period (04-11-2025 18:00 - 10-11-2025 07:00) is selected during which soil moisture at 10 cm depth is stable. Starting from this dry period, the cumulative rainfall is plotted against the change in soil moisture at 10 cm depth. The soil moisture signal is zeroed at the start of the period so that the vertical axis represents the change in soil moisture relative to the initial dry conditions. Under these conditions, incoming rainfall is first intercepted by the vegetation and stored in the upper soil layer before any soil moisture signal is detectable at 10 cm depth. The capacity is then estimated as the cumulative rainfall at the point where the soil moisture signal first exceeds the sensor noise threshold, as defined previously. This analysis is executed for the period 06-11-25 till 19-11-25. This is still before the pruning date so it captures the influence of the vegetation. This additional graphical approach is added as a check because it is less sensitive to threshold choices.

2.5. Water balance over the entire observation period

If all mass balance components of the water balance are can be determined the cumulative water balance over the entire observation period can be used to check for water balance closure. The goal is to calculate the cumulative evapotranspiration via the water balance and compare the outcome with the reference value for the cumulative evapotranspiration as described in section 2.3.1. The equation for the water balance over the entire period is equation 2.9. The entire observation period that ran from 17-10-25 up to 19-01-26.

$$ET_{cumulative} = P_{cumulative} - D_{cumulative} - \Delta S_{total} \tag{2.9}$$

Where:

- $P_{cumulative}$ is the cumulative precipitation over the entire period in mm
- $D_{cumulative}$ is the cumulative outgoing drainage over the entire period in mm
- ΔS_{total} is the storage change over the entire period in mm

If the the water balance in equation 2.9 can be closed or not, provides insights in if the mass balance components of the compartments are determined correctly.

3

Results and Discussion

This chapter presents and discusses the results of the methods to determine each water balance component. First the measured sensor data is analyzed and is checked for usability, this outlines which sensor data can be used. Then, the results for the precipitation component and outgoing drainage component are presented. After that, the attempts for quantifying the storage change component for the whole profile are shown. Since the main objective of this thesis is to determine the water demand of urban green spaces by solving the water balance, the components of the water balance are the primary results. For each component, it is therefore also directly discussed whether the results are usable. Lastly it is looked if the cumulative water balance over the entire period can be closed.

3.1. Sensor data quality check

Before presenting the results of the different analyses, the sensor data was first examined to verify that the measurements were consistent and behaved as expected. This is a basic quality check to confirm that the sensors were functioning properly during the observation period and that the recorded values are physically plausible. Reference values established in section 2.3.1 are also used for this. The sensor data is quality checked for all compartments and a judgment is made about the usability of the sensor data.

Sensor check compartment A

What can be noted about the sensor data of compartment A, seen in figure 3.1 is:

- All quantities for precipitation and soil moisture are in the right order of magnitude and consistent with the reference values established in section 2.3.1.
- The lower soil moisture sensor displays roughly the same pattern as the upper, but in general with a time delay.
- Most increases in soil moisture are preceded by precipitation events.
- During extended dry periods ~6-14 November), soil moisture gradually decreases.

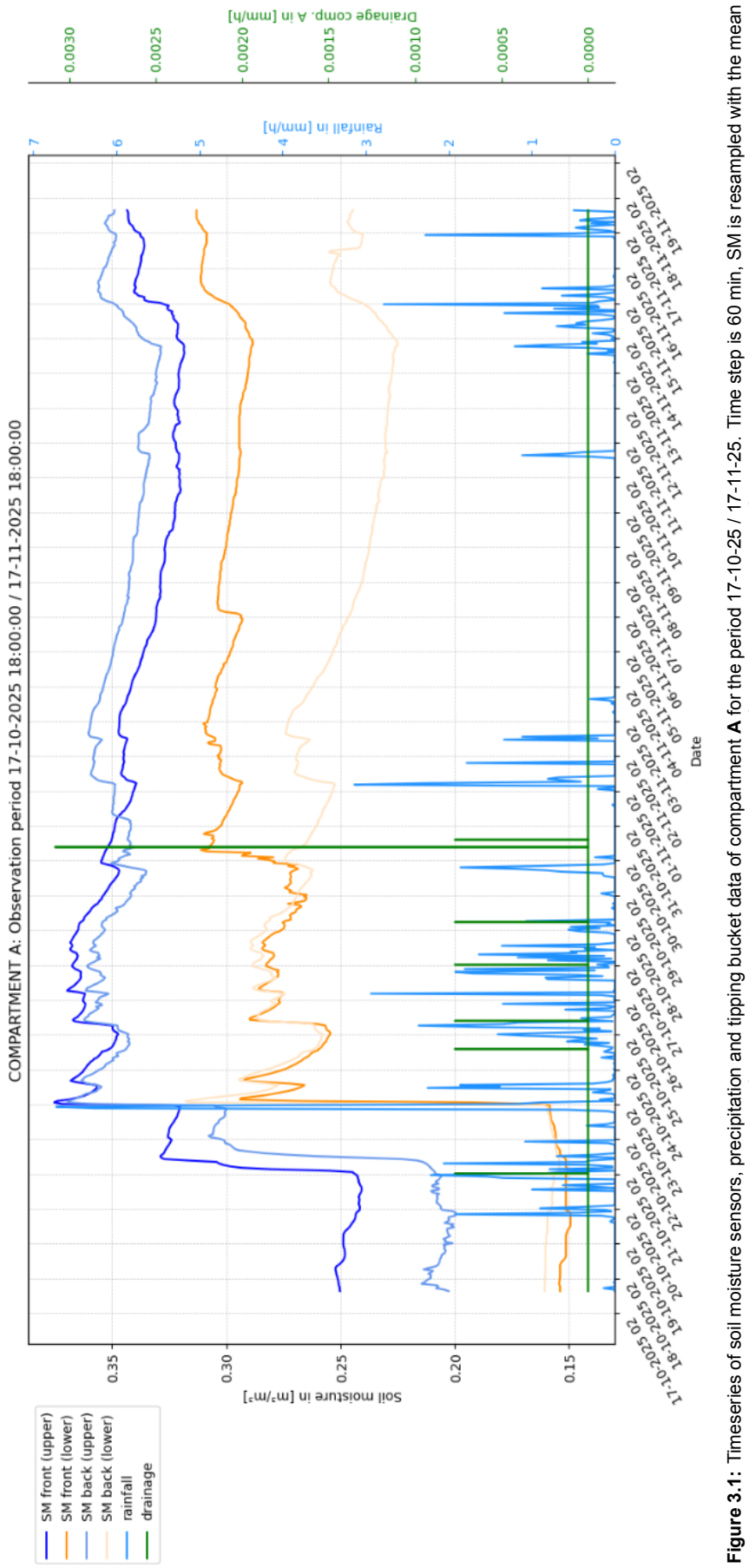

Figure 3.1: Timeseries of soil moisture sensors, precipitation and tipping bucket data of compartment **A** for the period 17-10-25 / 17-11-25. Time step is 60 min, SM is resampled with the mean and drainage and rainfall with the sum. The drainage values in this figure are over the area of the entire compartment.

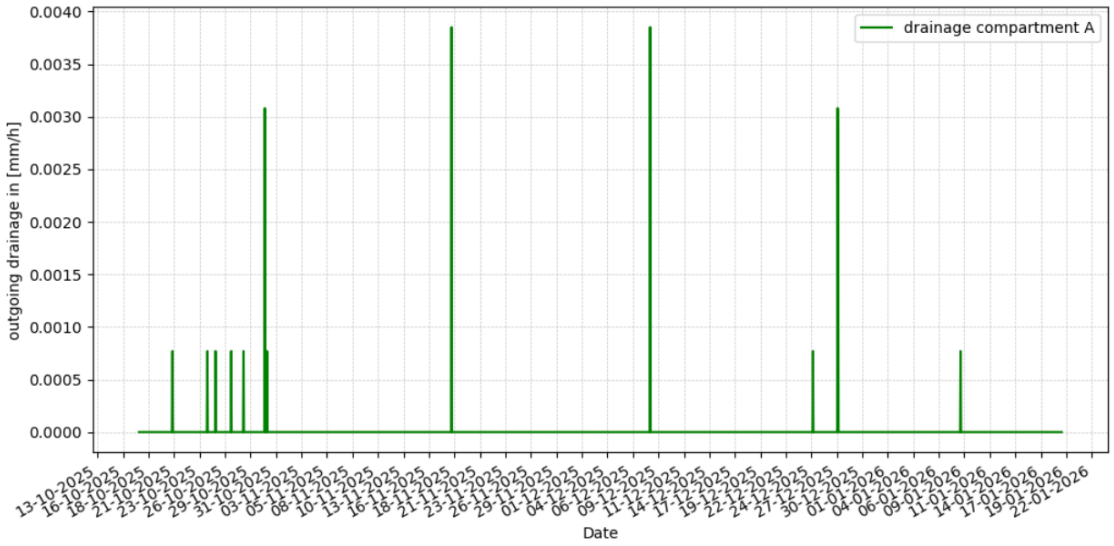

Figure 3.2: Outgoing drainage timeseries of the entire observed period of compartment A in mm. Resampled to 1 hour with the sum. The drainage values in this figure are over the area of the entire compartment.

For compartment A, there were limitations in the measurement of the outgoing drainage. The time series indicates almost no drainage except for some spikes at certain time stamps (see figure 3.2). Over the entire observation period the total outgoing drainage added up to 0.022 mm, which is too small. Two explanations for this lack of outgoing drainage are leakage and tipping bucket malfunctioning. Leakage is considered possible because the divers do not indicate a water level inside the compartment, so water has left the compartment undetected by the tipping buckets. This is either because of leakage through the plastic lining or through the seal between the under drain and the foundation walls or through the sealing between the outlet drain pipe and tipping bucket lid. The other explanation is that the tipping bucket of compartment A is malfunctioning and it can not register reliable drainage values. Which of these explanations is true is not determined

Sensor check compartment B

What can be noted about the sensor data of compartment B seen in figure 3.3

- All quantities for precipitation, outgoing drainage and soil moisture are in the right order of magnitude and consistent with the reference values established in section 2.3.1.
- The lower soil moisture sensor displays roughly the same pattern as the upper, but in general with a time delay.
- Most increases in soil moisture are preceded by precipitation events.
- After peak drainage events, the drainage signal gradually decreases over time. This is as expected with gravitational drainage
- Drainage events occur mostly after periods of rainfall and elevated soil moisture levels. When this is not the case this is an argument that storage / water retention is happening in the compartment.
- During extended dry periods ~6-14 November), soil moisture gradually decreases and drainage approaches zero, which is consistent with evapotranspiration and redistribution of water within the soil.

The lower soil moisture sensor that is located at the back of the compartment displays fluctuations exceeding what can be attributed to typical sensor noise, as illustrated in figure 3.4. These spikes are attributed to sensor failure. This makes the sensor values of the lower soil moisture sensor in the back of compartment B not usable.

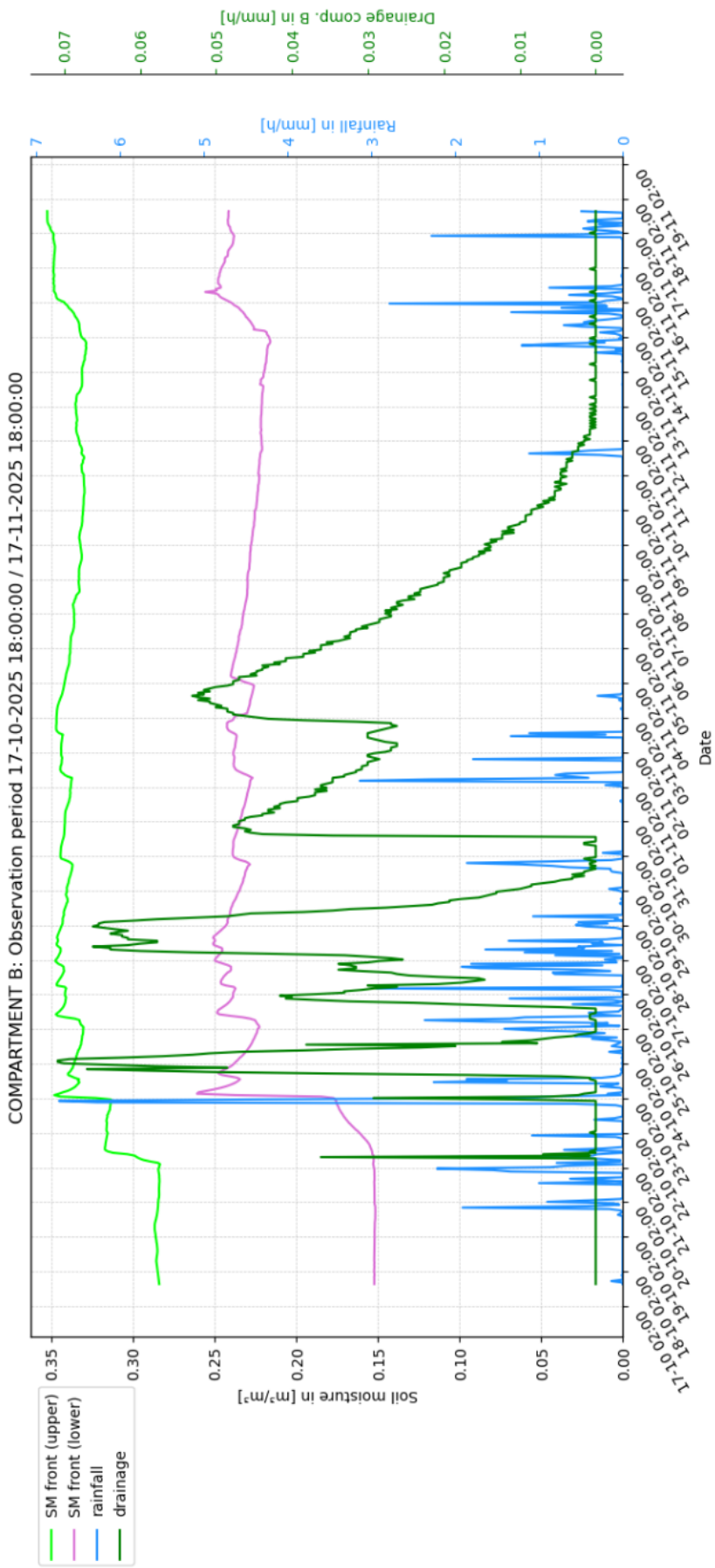

Figure 3.3: Timeseries of soil moisture sensors, precipitation and tipping bucket data of compartment **B** for the period 17-10-25 / 17-11-25. Time step is 60 min, SM is resampled with the mean and drainage and rainfall with the sum. The drainage values in this figure are over the area of the entire compartment.

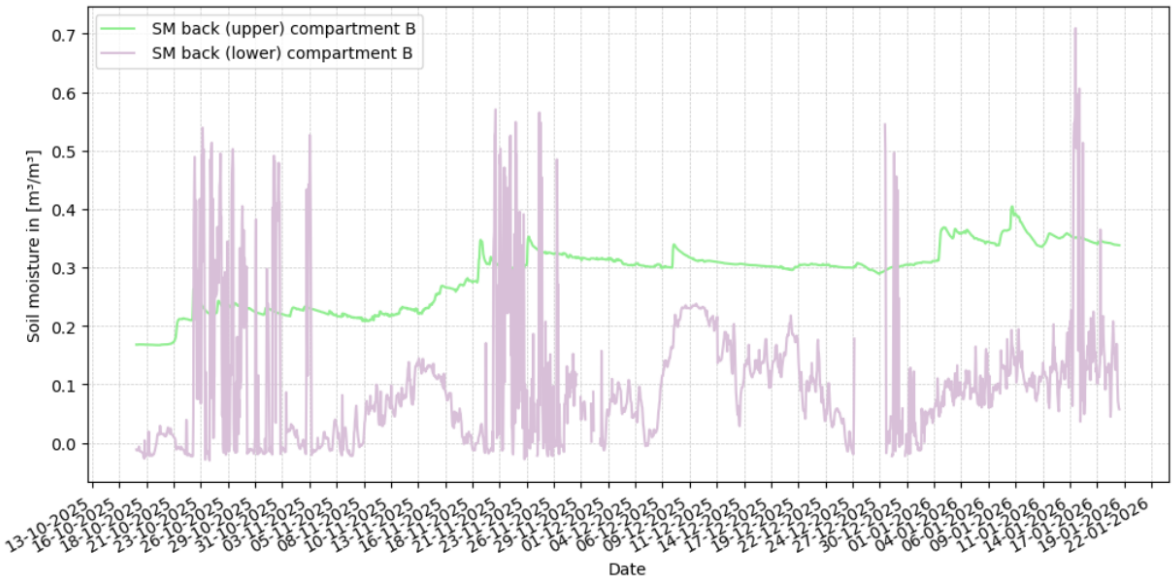

Figure 3.4: Timeseries of soil moisture sensors of the entire observed period of *the back* of compartment B in m³/m³. The values are in a 1 hour time resolutions

The time series from the sensors of compartment B that are plotted in figure 3.3 indicate that the sensors functioned consistently and provide measurements which can be used for a water balance model. Soil moisture dynamics and drainage responses are behaving as expected and magnitudes are in agreement with the reference magnitudes established in section 2.3.1. Only soil moisture sensors in the front of the compartment can be used since there is malfunctioning of one of the sensors in the back.

What can be noted about the sensor data of compartment C seen in figure 3.5 is:

- All quantities for precipitation and soil moisture are in the right order of magnitude and consistent with the reference values established in section 2.3.1.
- The lower soil moisture sensor displays roughly the same pattern as the upper, but in general with a time delay
- Most increases in soil moisture are preceded by precipitation events.
- During extended dry periods ~6-14 November), soil moisture gradually decreases.

For compartment C, there is also sensor behavior that is not expected. The outlet drain is configured in such a way that the tipping bucket should only register drainage values when the water level in compartment C exceeds 50 cm (see sub-figure 2.3b). Despite this outlet drain configuration, the divers in compartment C that check whether there is a water table do not show a water level build up inside the compartment. This indicates that compartment C has leakage either through the plastic lining or through the seal between the under drain and the foundation walls or in the outlet drainage pipe.

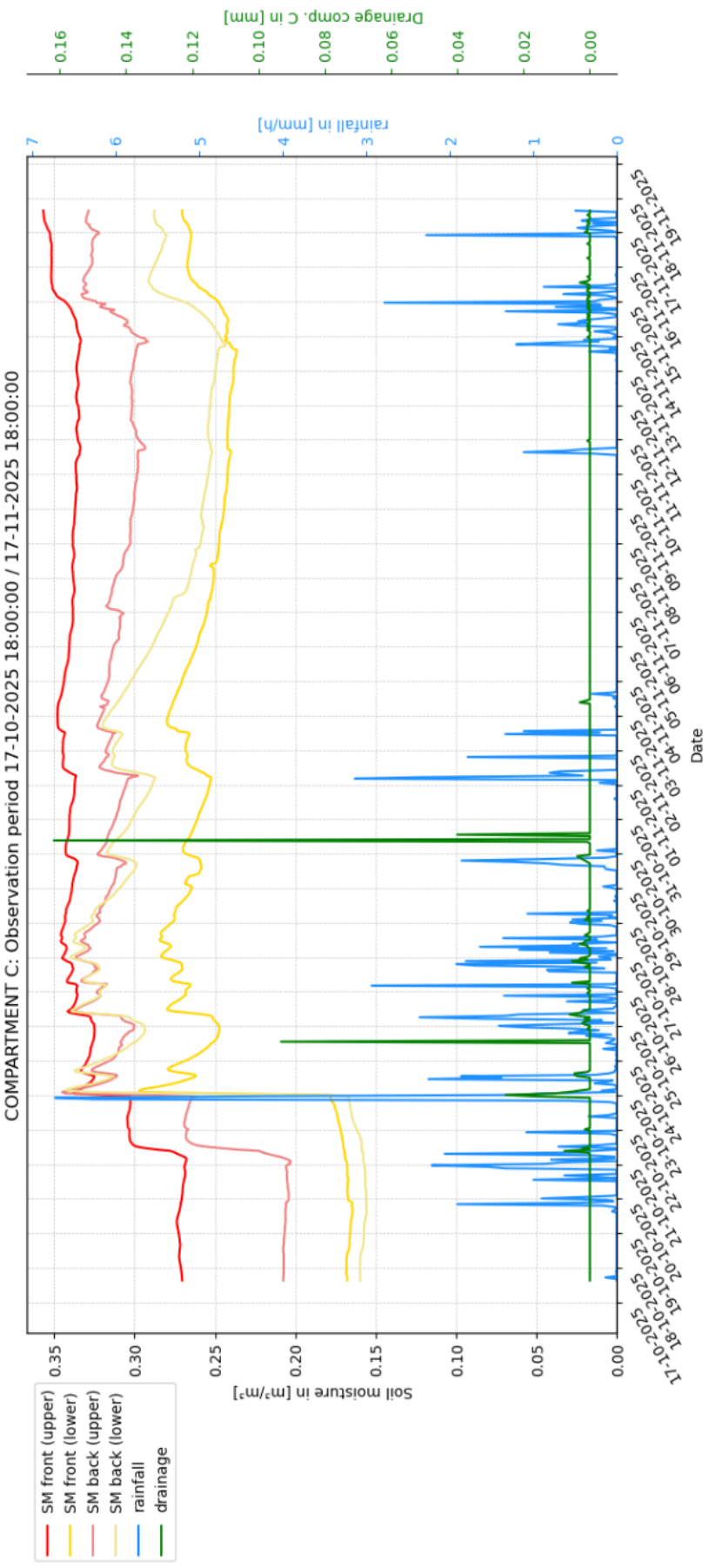

Figure 3.5: Timeseries of soil moisture sensors, precipitation and tipping bucket data of compartment **C** for the period 17-10-25 / 17-11-25. Time step is 60 min, SM is resampled with the mean and drainage and rainfall with the sum. The drainage values in this figure are over the area of the entire compartment.

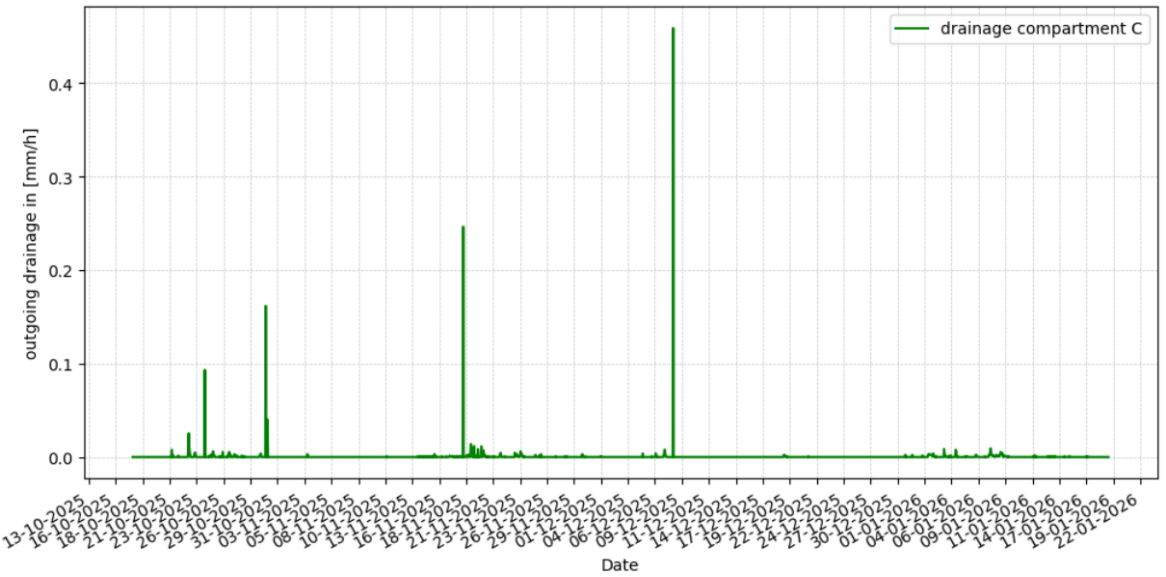

Figure 3.6: Outgoing drainage timeseries of the entire observed period of compartment C in mm/h. Resampled to 1 hour with the sum

Despite this leak figure 3.6 shows values. It shows a maximum drainage peak of 0.45 mm/h. The compartment area was 5.22 m^2, so this peak corresponds to 0.00045 m $\cdot$ 5.22 m^2 = 2.35 L of water. With the tipping bucket spoons having 4.02 mL/tip, this translates to 2.35 / 0.00402 = 584 tips. Therefore, the possibility that caused by mechanical movement of the housing of the tipping bucket is ruled out. Since the tipping bucket is elevated further from the ditch than those of compartments A and B, water entering from below cannot be the cause of these tips. A more likely cause of this outgoing drainage measurement and by the same logic also the smaller ones, is that the lids of the tipping buckets are not fully sealed. Water may accumulate on the lids and leak through the space between the lid and the outlet pipe of the compartment. That together with measurement noise can cause the registration of outflow when there should not be any.

3.1.1. Statement about snow processes and frozen soil conditions

Snow accumulation and frozen soil conditions introduce processes that are not explicitly accounted for in this thesis. When snow accumulates on the surface, the actual water input to the compartments is delayed until the snow melts. Also, frozen soil conditions can reduce infiltration capacity, delaying the movement of water through the soil profile. However, these processes are not expected to affect the conclusions of this project. For the cumulative water balance over the entire observation period, the timing of water input is not important since all accumulated snow will eventually melt and enter the system as liquid water. For the outgoing drainage component, any delayed infiltration or snowmelt-driven drainage would occur near the end of the observation period, where the tipping bucket data of compartment B already shows near-zero drainage, meaning the effect on the cumulative drainage is negligible. For the nighttime water balance analysis, the snow and frozen soil conditions could introduce timing inconsistencies between the recorded precipitation and the observed storage response during the affected nights. However, this analysis is used to evaluate trends in water balance closure rather than quantifying exact quantities. Lastly, the days of snow and freezing are approximately 9 days and are a small fraction of the total 94-day observation period. For these reasons, snow accumulation and frozen soil processes are not explicitly included.

3.2. Results of the mass balance components

Section 3.1 showed that compartment A and compartment C have unreliable outgoing drainage values. Therefore they can not be used to apply the mass balance method on and obtaining a reliable estimate for the evapotranspiration term. Compartment B showed sensor values that are possible and the outgoing drainage value of compartment B does not have the same unexpected behavior as compartments

A and C. It it therefore chosen to apply the methods for determining the mass balance components, as described in section 2.4, only to the dataset of compartment B. The results described in the current section will mainly be focused on compartment B.

3.2.1. Precipitation component

The precipitation data for the observation period was obtained directly from the weather station at Green Village. During this period, the majority of precipitation fell in the periods 20-10-25 / 28-10-25 , 13-11-25 / 25-11-25 and 02-01-26 / 10-01-26. Like stated in subsection 2.4.2, no irrigation was applied, so all water inputs to the compartments originate from precipitation. These measurements serve as the primary input for the water balance calculations. Figure 3.7 provides an overview of the rainfall amount and the cumulative rainfall of the entire observation period. There is uncertainty in the analysis made with precipitation because of the difference in precipitation values between the data from the Green Village station and the Rotterdam Airport station, mentioned in section 2.3.1.

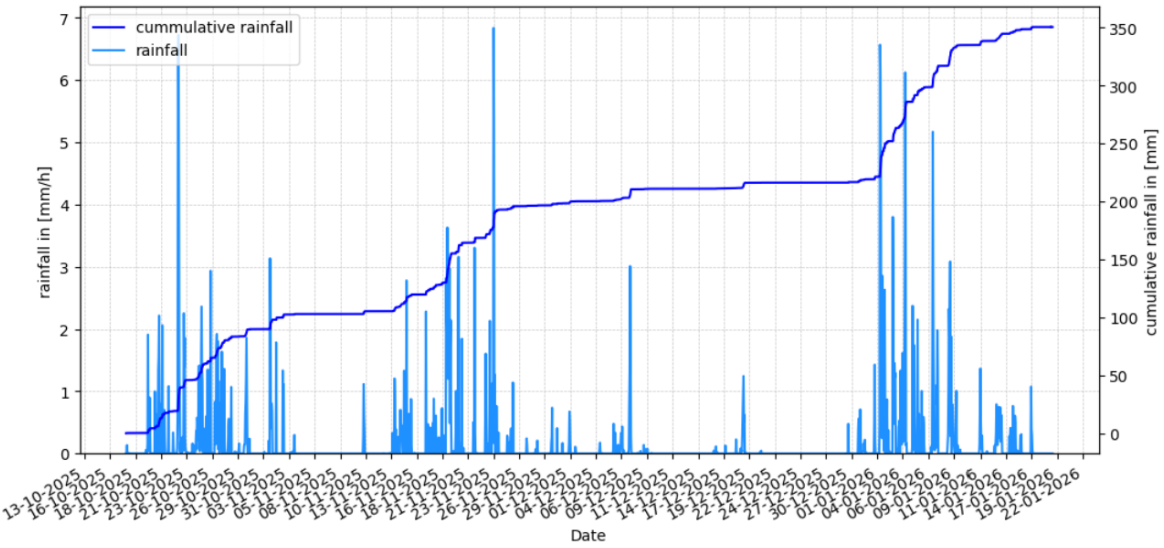

Figure 3.7: Time series plot of the cumulative rainfall and the rainfall of the entire observation period in mm. Rainfall is resampled to 1 hour with the sum

3.2.2. Outgoing drainage component

Like stated earlier outgoing drainage measurements in compartments A and C are unreliable because of leakage and or tipping bucket malfunctioning. Figure 3.8 shows the time series of the outgoing drainage of compartment B. When drainage occurs, it would normally be visible over multiple consecutive time steps and would show a gradual increase and decrease, which is observed in compartment B. The cumulative drainage over the entire observation period for this compartment is 51.8 mm, which is below the bound established in section 2.3.1. So if storage change over the observation period is larger than zero, the 51.8 mm is in agreement with the outgoing drainage bound. The outgoing drainage values of compartment B are considered usable for the mass balance method.

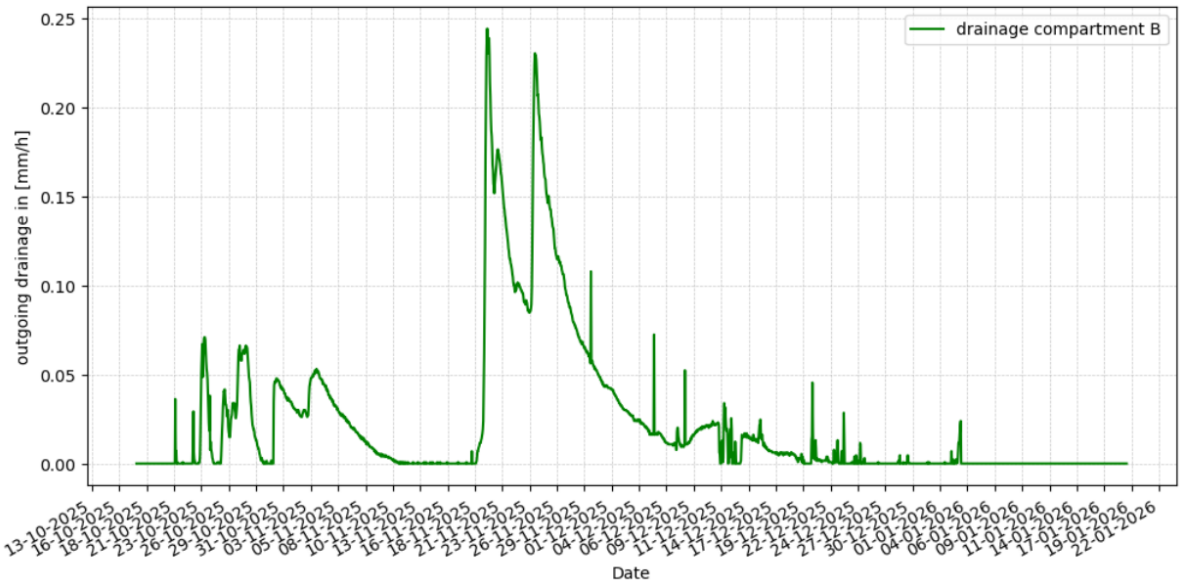

Figure 3.8: Time series plot of the outgoing drainage of compartment B for the entire observation period. Resampled to 1 hour resolution with the sum. The drainage values in this figure are over the area of the entire compartment.

3.2.3. Storage change components

Storage change is not directly measured by the instrumentation and therefore must be estimated using the soil moisture observations and different analytical approaches. Storage change is not quantified for the whole soil profile. This section describes the results of estimation of partial storage changes in the top soil layer. Also, the night time balance closure results are presented here together with the results of the estimation of lower bound of water storage on vegetation and first 10 cm of soil and the time lag between soil moisture sensor signals.

Upper layer storage dynamics results

This section discusses the results of the storage estimation in the upper 0.35 m of soil of MeSUDa.Figure 3.9 shows the linear soil moisture profiles based on equation 2.3 for three representative soil moisture conditions in compartment A: a dry period, an after-rainfall moment, and an intermediate state. Appendix figures A.2 and A.3 provide the other soil moisture profiles of the other compartments.

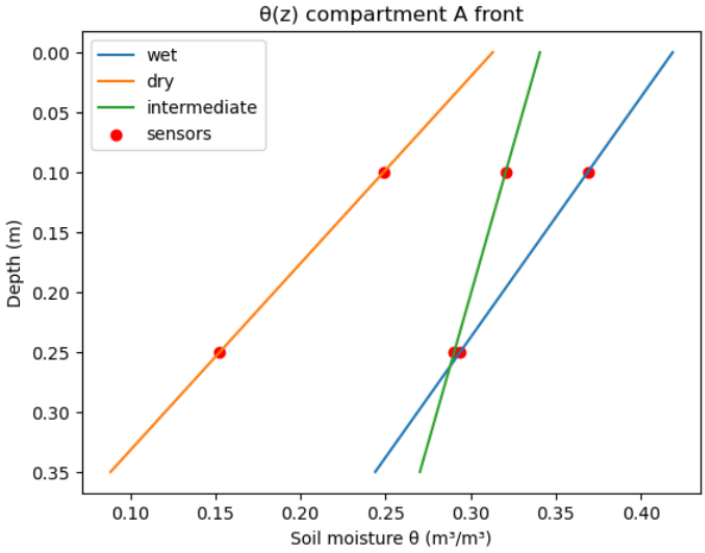

Figure 3.9: Linear soil moisture profiles θ(z) for the first 0.35 m of upper soil, based on soil moisture measurements of three representative periods. This one is from compartment A.

The time series of the storage estimation according to equation 2.4 for the whole observation period is plotted in figure 3.10.

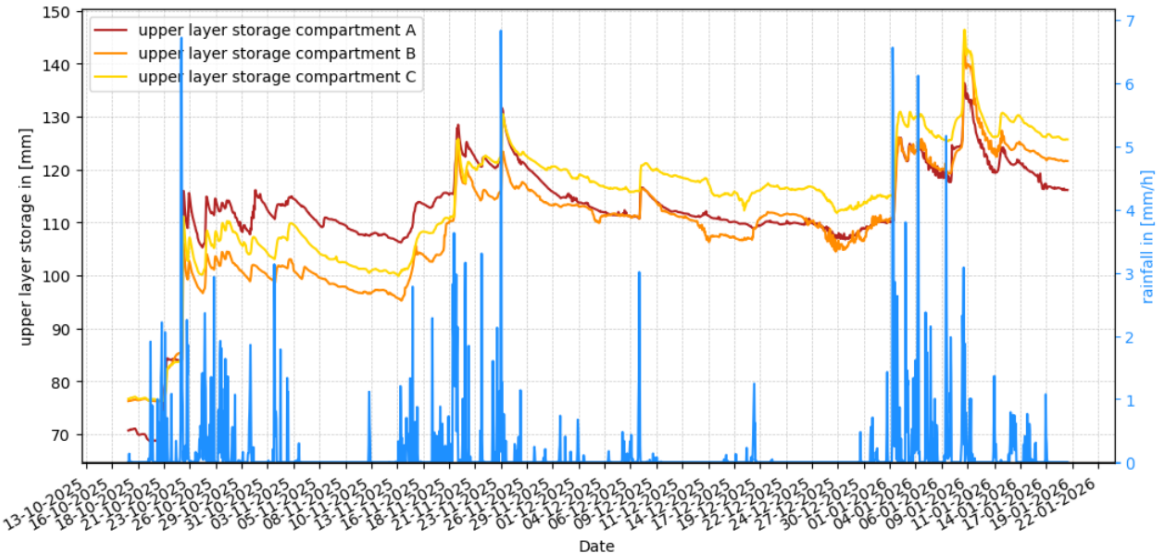

Figure 3.10: Timeseries of the storage estimates for the upper 0.35 m of soil for each compartment for the entire onservation period. Rainfall in mm/h. The time resolution of the soil moisture sensors where this estimation was based of was 1 hour

As can be seen in figure 3.10 the increases in storage correspond to rainfall events, while gradual decreases correspond to soil drying due to evapotranspiration and drainage. Compartment C generally shows higher storage values than compartments A and B. The differences between the estimated upper layer storage between the last observation day and the first observation day are: 45.4 mm for compartment A, 45.4 mm for compartment B and 49.0 mm for compartment C. So all the storage values increased over the observation period. Note these increases are only of the estimation for water storage in the upper layer of the compartment not of the whole profile. So, what can be said is that the change in storage in the upper layer is not equal to zero over the observation period, i.e. $\mathrm{dS_{upper}}/\mathrm{dt} \neq 0$. And because this only applies to the upper layer, it does not necessarily mean that the storage change over the entire soil profile cannot be zero.

The assumption of the linear interpolation and extrapolation of the soil moisture profile between and beyond the two sensor depths (equation 2.3) affects the results for estimation of the upper layer storage. The sensors are placed at 10 cm and 25 cm depth, but the linear trend is extrapolated downward to 35 cm and upward to 0 cm. The extrapolation to 0 cm is critical, because the topsoil close to the surface is where the most dynamic moisture changes happen like evaporation, rainfall interception and wetting fronts. If the actual soil moisture near the surface deviates from the assumed linear profile (for example, if it is much drier due to surface evaporation or much wetter immediately after rainfall), the estimated storage S(t) from equation 2.4 will be wrong. This affect also all subsequent conclusions that are drawn with the upper layer storage.

Results night time water balance analysis

The nighttime water balance was evaluated by comparing the net input $P_{night} - D_{night}$ with the observed storage change for each night. Figure 3.11 shows a scatter plot of these variables for compartment B, together with the 1:1 reference line. Important to note that the storage mentioned in this subsection, is the same storage as defined in sub subsection ”Upper layer storage dynamics results”. Each dot represents a night of the data set and the colored bar on the right of the figure shows the upper layer storage level at the beginning of the night, the ”antecedent storage”.

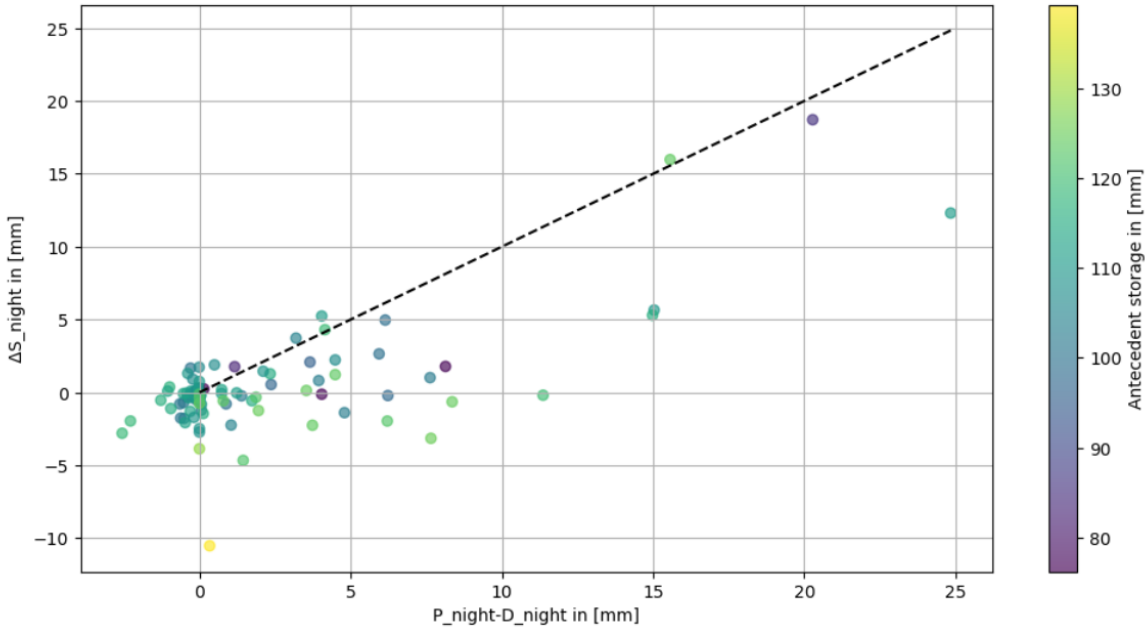

Figure 3.11: Scatterplot of the net input in mm v.s. the change in upper layer storage over the night in mm of compartment B. The colored bar indicates the upper layer storage value at the beginning of each night

Most points in the scatter plot lie below the 1:1 line, this indicates that the observed nighttime storage change ΔS_{night} is generally smaller than the net input $P_{night} - D_{night}$. This suggests that not all infiltrating water is captured within the upper layer storage, with some water likely redistributing to deeper layers of the soil profile. Also, a cluster of points with $P_{night} - D_{night}$ shows negative ΔSnight, implying that downward redistribution within the soil dominates even in the absence of net rainfall or drainage. Overall, the upper layer storage dynamics reflect local wetting and drying patterns rather than the full soil profile response. This is confirmed by scatterplots of compartment A and C, these can be found in appendix figures A.4 and A.5.

Results estimation of time lag between the two soil moisture sensors

The time relationship between the upper and lower soil moisture sensors was evaluated using two approaches: cross-correlation and dynamic time warping (DTW). The aim was to quantify the time lag in water propagation from the upper to the lower soil moisture sensor. This is to quantify the travel time of water through the top soil and thereby estimating when it leaves the top soil layer and moves into the fine sand layer. This could help constrain the storage change for the deeper parts of the soil profile. Rainfall events were also considered to contextualize variations in soil moisture response.

The cross-correlation approach was performed on the differenced and mean-centered soil moisture time series. The cross-correlation method provides a statistical estimate of the lag. To evaluate the sensitivity of the cross-correlation approach to the time resolution of the soil moisture data, the analysis was repeated for a range of time resolutions between 1 minute and 180 minutes. Table 3.1 gives the time resolutions of the soil moisture sensors of compartment B and the calculated time lags with their correlation values.

Table 3.1: Correlation and time lag for selected time resolutions of compartment B.

Time resolution	Time lag [min]	Correlation [-]
1 min	7.0	0.07
5 min	35.0	0.07
15 min	45.0	0.22
30 min	60.0	0.38
45 min	45.0	0.44
50 min	50.0	0.47
60 min	60.0	0.54
120 min	120.0	0.63
180 min	180.0	0.59

At high time resolution (5 minutes), the correlation between the two soil moisture signals is very low (0.07), and the estimated lag (≈ 35 minutes) is not considered reliable. This indicates that the signals are dominated by high-frequency variability and sensor noise.
At lower time resolutions (15–60 minutes), the correlation increases (up to 0.54), while the estimated lag stays between approximately 45 and 60 minutes. This suggests that lower time resolutions reduce noise and become more suited as signals for the cross-correlation to estimate the time of the vertical movement of water between the two soil moisture sensors. At even lower resolutions (120–180 minutes), the correlation further increases (up to 0.63), but the estimated lag also increases to 2–3 hours. This is interpreted as that the time aggregation of the soil moisture signals artificially delays the apparent response of the lower sensor. As a result, the lag is overestimated at these resolutions.

It is also observed that for some time resolutions, the estimated time lag is equal to the resolution itself (e.g. 60 minutes at 60-minute resolution, and 120 minutes at 120-minute resolution). This is because the cross-correlation works with discrete time steps, so the lag is limited to multiples of the chosen time resolution. Therefore, these results should be interpreted as order of magnitude values of the lag and not as exact values.

The DTW approach provides a time-dependent estimate of the lag between the two soil moisture signals. DTW can account for varying response speeds. The DTW algorithm was applied to the upper and lower soil moisture time series for the entire observation period. Figure 3.12 shows the resulting time lag signal of compartment B, together with the rainfall record and the original soil moisture signals . Several features of the lag signal are to be interpreted carefully.

The most physically meaningful periods are the ones following precipitation events because there the soil moisture signals react after each other to the infiltrating rain water. Based on the saturated hydraulic conductivity of the topsoil of k_{sat} = $1.4 \cdot 10^{-5}$ m/s [29], [30] and the vertical distance of 15 cm between the two sensors, a range of the time lag is estimated to be between 0 and approximately 180 minutes. The lower bound of 0 corresponds to the case where the soil is already saturated and both sensors respond at the same time. The upper bound is obtained by dividing the distance between sensors by k_{sat}, giving the slowest realistic travel time under saturated conditions. The lag values observed in the signal however frequently exceed this range, which indicate that the DTW-derived lag does not reliably capture true wetting front speed. A zoomed in version of figure 3.12 is given in figure 3.13, where the theoretical range of the time lag is given based on saturated conductivity.

These unrealistic values come from a fundamental limitation of the global DTW alignment: the algorithm optimizes a single warping path across the entire time series simultaneously, without any constraint on the direction or magnitude of the lag [45]. During dry periods or gradual seasonal transitions, the two soil moisture signals can evolve quite differently from each other. Since DTW must match every point in one signal to some point in the other, it is forced to find a partner for each point regardless of whether a meaningful physical relationship exists. In these periods, the algorithm will therefore match points that are far apart in time simply because they are the closest available match, producing lag values that show the mathematical constraints of the warping method instead of any real hydrological process. Negative lags, in which the lower sensor appears to respond before the upper one, occur when the

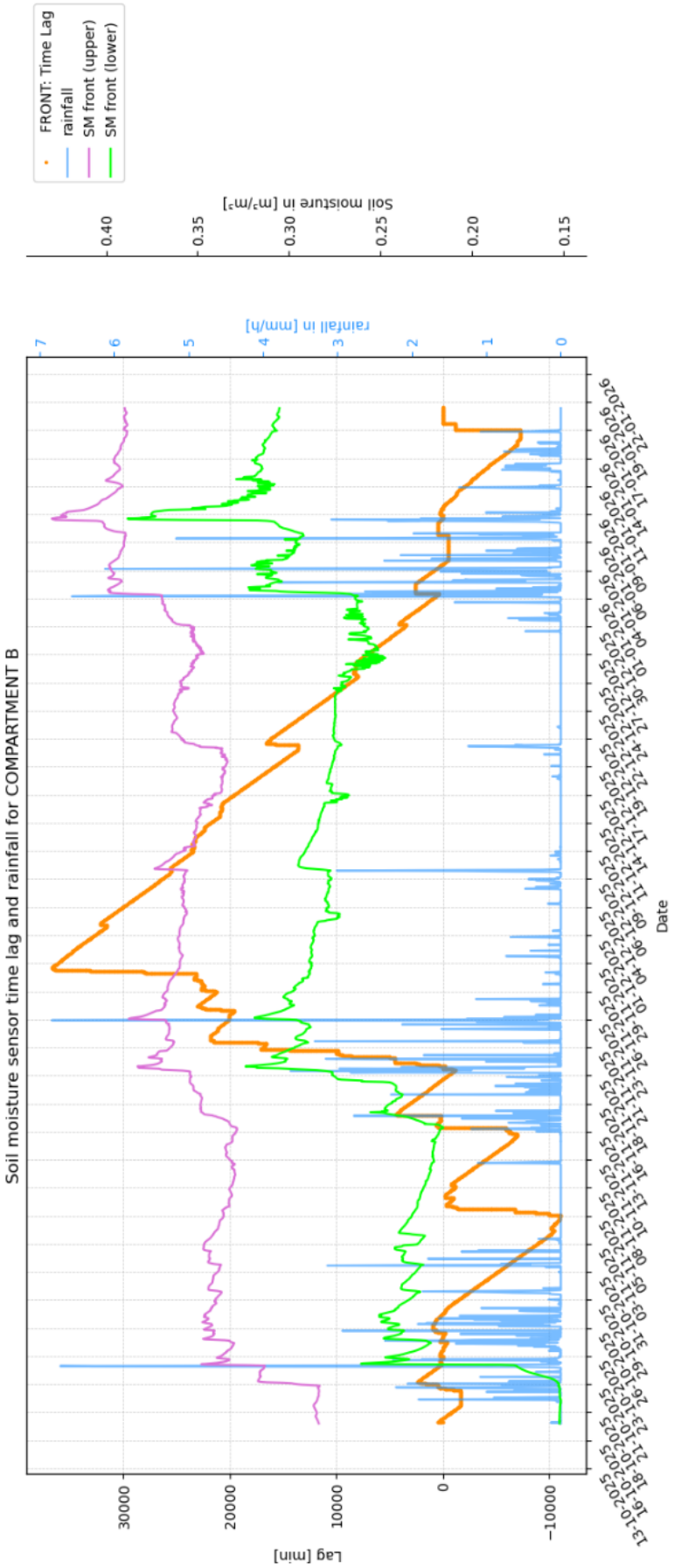

Figure 3.12: Time lag evolution between the two soil moisture sensors of compartment B in minutes for the whole observation period. The rainfall and the soil moisture sensors signals are also plotted in the figure in mm and m³/m³ respectively all in 1 hour time resolution

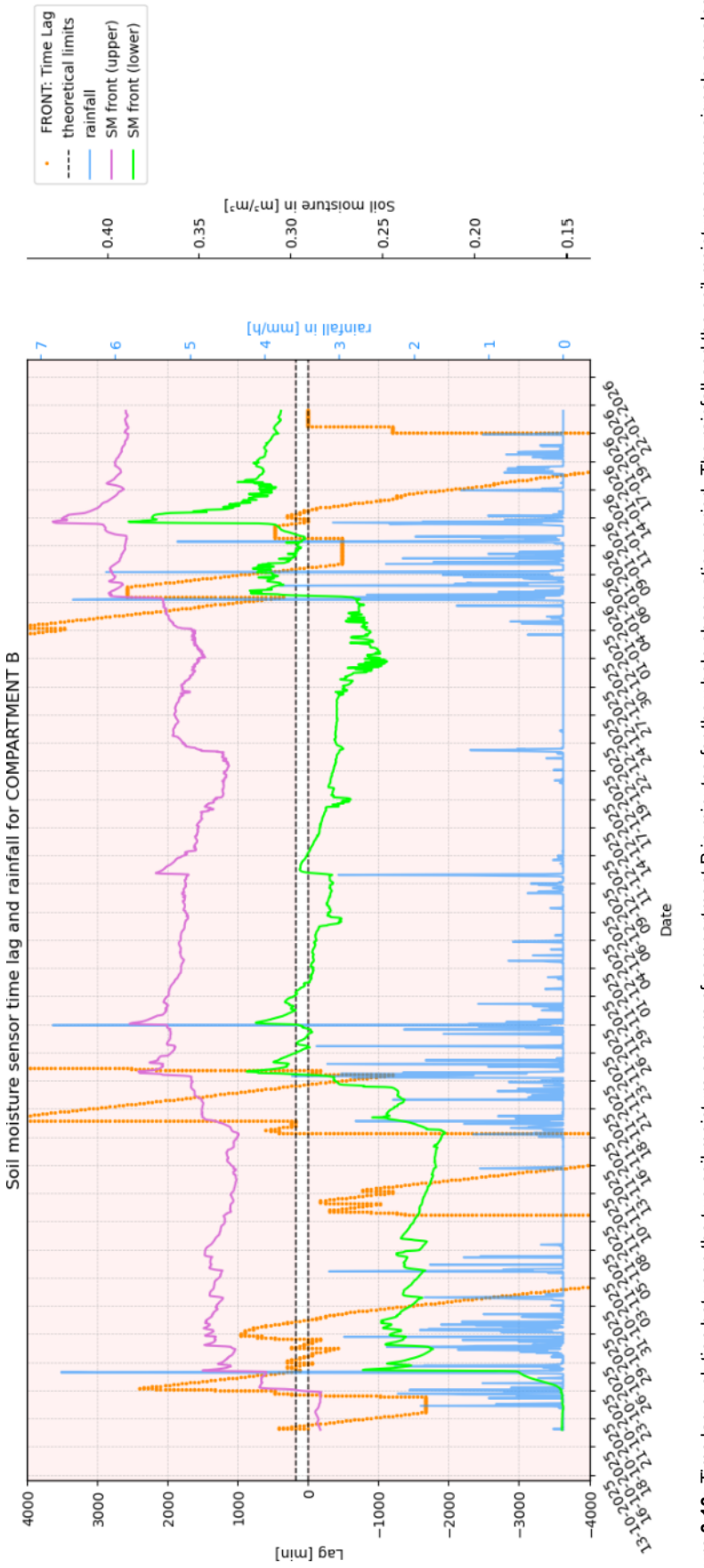

Figure 3.13: Time lag evolution between the two soil moisture sensors of compartment B in minutes for the whole observation period. The rainfall and the soil moisture sensors signals are also plotted in the figure in mm and m^3/m^3 respectively all in 1 hour time resolution. A theoretical time lag range

lower sensor keeps elevated moisture from a prior event while the upper sensor has already dried, leading to a reversed alignment that has also no physical meaning.

All together, these results indicate that the DTW approach as implemented here does not produce physically interpretable lag estimates for this dataset. The absence of a constraint on the warping path length and direction allows the algorithm to generate alignments that are mathematically optimal but physically meaningless.

Results quantifying lower bound estimate of water storage on vegetation and first 10 cm of soil

The event-based rainfall threshold analysis to quantify the lower bound of water storage on vegetation and first 10 cm of soil is applied on the data of each compartment. The results can be seen in table 3.2. Like stated in section 2.4.5, the total observation period is split around the pruning date of 30-11-2025. What can be seen in table 3.2, is that all the estimated lower bounds after cutting the plants, are higher than before cutting the plants. This is a counterintuitive result, because that means that the lower bound estimated water stored on vegetation and first 10 cm of soil is larger after the removal of plant than with plants. Therefore, these results must be interpreted carefully.

Table 3.2: The lower bound estimates of the water storage on vegetation and first 10 cm of soil before, after pruning and of the plants of all compartments of MeSUDa, all in mm

	$I_{before,prune}$ [mm]	$I_{after,prune}$ or I_{soil} [mm]	I_{plants} [mm]
compartment A	3.14	11.23	-7.09
compartment B	2.49	11.23	-6.74
compartment C	2.81	3.64	-0.83

The most likely explanation for this counterintuitive result, lies in the nature of the lower bound estimation method itself. The method is sensitive to which rainfall events happen to occur within a given period. If no sufficiently large rainfall event qualifies as a non-responsive rainfall event in a given period, the lower bound will be artificially low, independent of the true physical capacity. The period before the pruning is shorter and contains fewer events, which reduces the probability that a large non-responsive rainfall event is present in the dataset, and therefore likely underestimates the true capacity for that period.
In addition to the lack of data, antecedent soil moisture conditions likely differ between the two periods. Before the cut, soils may have been wetter due to earlier autumn rainfall, meaning that even moderate rainfall events were enough to produce a detectable soil moisture response at 10 cm. This would push events out of the non-responsive rainfall category and would decrease the estimated maximum. After the cut, if the soils were drier on average, more events would satisfy the no-response filter because the soil has more available pore space to absorb incoming water. This is also true for the larger rainfall events, so this makes the estimated lower bound for that period larger.
Also, there is the difference in rainfall event characteristics between the two periods. If the events before the pruning date were on average more intense or longer, they would be more likely to exceed the threshold and therefore less likely to qualify as non-responsive rainfall events, again making the estimated capacity artificially lower
Taking this all in consideration, this also explains the negative values for I_{plants} in table 3.2. Just because of the way equation 2.7 was constructed.

Given these considerations, a direct comparison of the before and after estimates to derive a lower bound estimate for the water storage on the vegetation and the water stored in the first 10 cm of soil is not straight forward and this method is not suited to give an estimation for the storage capacity on the plants.

Results graphical approach

Figure 3.14 shows the result of the graphical method for the estimation of the amount of rainfall required to reach the upper soil moisture sensor depth for compartment B. This estimation was based on a time period from 6 November 2025 to 19 November 2025, which was before the pruning date of the plants. The cumulative rainfall is plotted on the horizontal axis and the zeroed soil moisture change at 10 cm depth on the vertical axis.

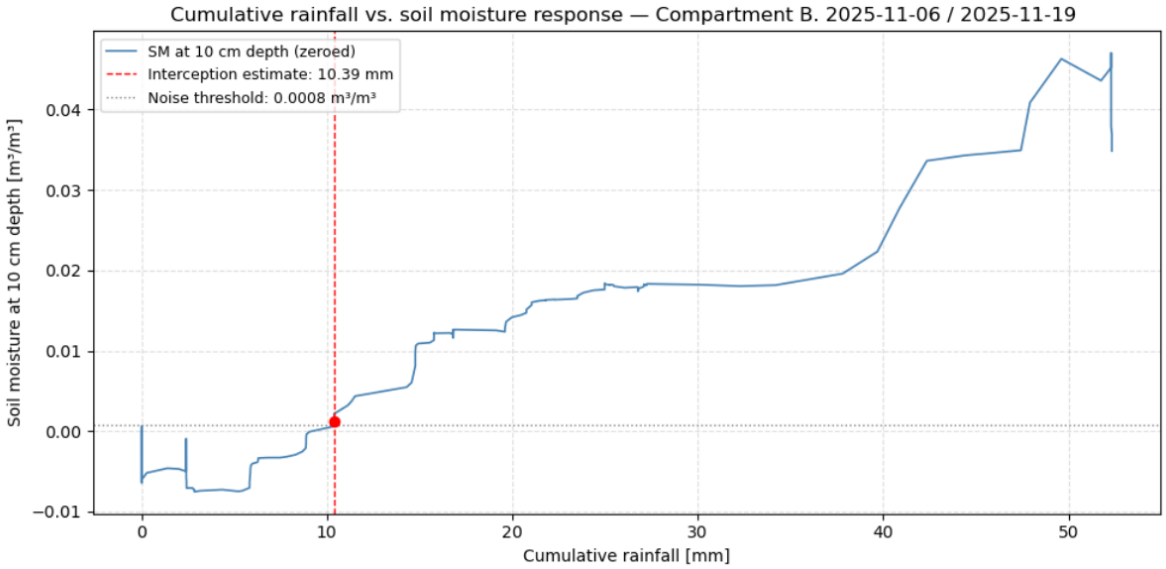

Figure 3.14: Cumulative rainfall v.s. the zeroed soil moisture level at 10 cm depth in [mm] and [m³/m³] respectively. This is for compartment B in period 06-11-25 till 19-11-25

During the first approximately 10 mm of cumulative rainfall, the soil moisture signal remains near zero and shows only small fluctuations indicating that incoming rainfall is being intercepted before reaching 10 cm depth. At a cumulative rainfall of 10.39 mm the signal first exceeds the noise threshold of 0.0008 m³/m³, which is indicated by the red dashed line and marker in the figure. For this graphical approach, this value is therefore taken as an estimate of the amount of rainfall required to reach the upper soil moisture sensor depth. The estimations according to this graphical approach for compartment A and C are 14.78 mm and 10.39 mm respectively and their figures can be found in appendix figures A.6 and A.7.

The same graphical method has been done fore a post-pruning period running from 21-12-2025 till 03-01-2026. This is also a dry period followed up by rainfall event(s). The result is seen in figure 3.15

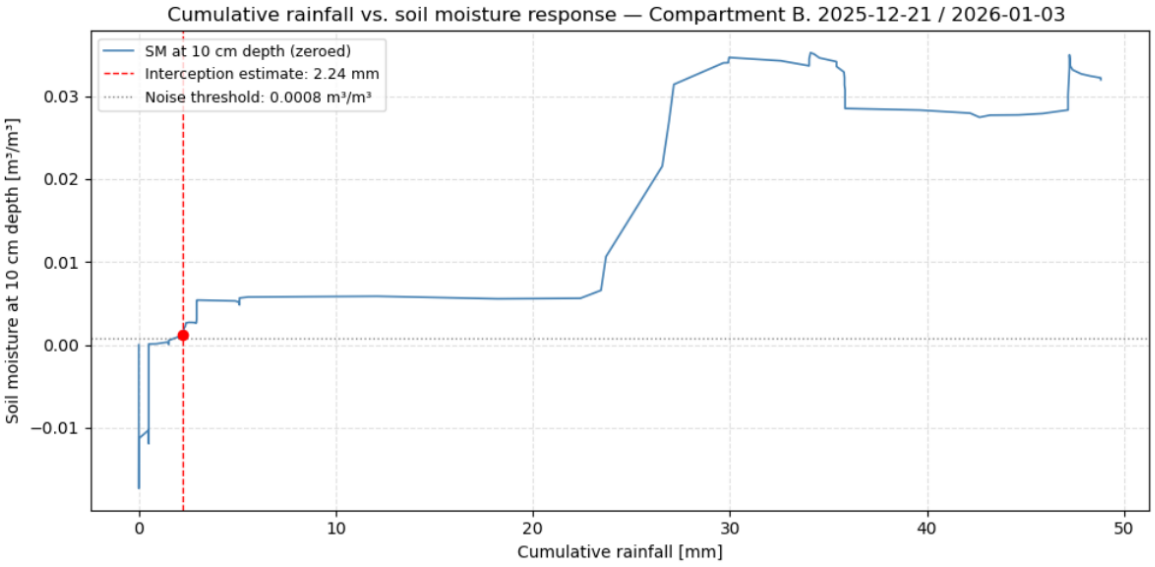

Figure 3.15: Cumulative rainfall v.s. the zeroed soil moisture level at 10 cm depth in [mm] and [m³/m³] respectively. This is for compartment B in period 21-12-25 till 03-01-26 (post-pruning)

In this case the estimate for the capacity of only the first 10 cm of soil is 2.24 mm, since it was post-

pruning so no water could be stored on the plants. The capacity of the storage on the plants can then be calculated as the graphical method estimate of the storage on the plants and first 10 cm of soil (so pre-pruning) minus the graphical method estimate of storage in only the first 10 cm of soil (so post-pruning). For compartment B this would become 10.39 mm - 2.24 mm = 8.15 mm.

Comparing the graphical estimate for the pre-pruning period to the pre-pruning lower bound estimates obtained from the event-based classification method in table 3.2, which were 3.14 mm, 2.49 mm and 2.81 mm for compartments A, B and C respectively, a difference is observed. The graphical method produces estimates that are approximately three to five times higher than the event-based estimates for the same pre-pruning period. This difference is not necessarily a contradiction between the two methods, but rather reflects the fundamental limitation of the event-based method that was already identified (the pre-pruning period is relatively short and contains fewer qualifying rainfall events, which reduces the probability that a sufficiently large non-responsive event is present in the dataset). The graphical method is based on one period of drought followed by cumulative rainfall, it does not rely on the classification of individual events and is therefore less sensitive to this limitation .

It should also be noted that the graphical estimate is sensitive to the soil moisture levels in the soil layer above the sensor at the start of the selected dry period. If the soil moisture levels above the 10 cm sensor differs per compartment, the same cumulative rain can trigger a different soil moisture response. This is because if this 10 cm is wetter, there is less space to store the water in before it reaches the soil moisture sensor at 10 cm depth. This is an explanation for the different results for the lower bound estimate of the water storage on the vegetation and the first 10 cm of soil between compartments according to the graphical method and the reason for underestimation of water storage in the first 10 cm of soil. This underestimation leads to an estimate for the storage capacity on the plants that is too high.

The goal of these analyses was to isolate the amount of water on the plants and further quantify the storage change component. Because of reasons discussed above this analysis was unsuccessful. It should be noted that even if this analysis gave reliable results, this would provide with a lower bound for the storage capacity on the plants and not the storage change on the plants for each time step.

Concluding statement storage change component

Although several approaches were explored to (partially) characterize storage change in the system, the storage change for the entire soil profile is not quantified in this project.

3.3. Results water balance over the entire observation period

The cumulative water balance over the entire period provides insights in if the mass balance components of the compartment are determined correctly. Like stated before the storage change is not quantified for the whole soil profile. Table 3.3 shows the results of the cumulative water balance over the entire observation period for compartment B according to equation 2.9 under the assumption that the net total storage change over the entire period is 0, e.g. ΔS_{total} = 0. The ET value presented in table 3.3 is not a physical measurements but the rest term of the water balance under the assumption that net storage change over the entire compartment is zero.

Table 3.3: Water balance over the entire observation period for compartment B according to equation 2.9.

	$P_{cumulative}$ [mm]	$D_{cumulative}$ [mm]	$ET_{cumulative}$ [mm]
compartment B	350.6	51.8	298.8

The results of this water balance can be compared with the reference value as described in section 2.3.1. There, the cumulative evapotranspiration over the entire period showed a value of 42.8 mm. This is far lower than the evapotranspiration value presented in table 3.3. This can be an indication that the assumption that $\Delta S_{total} \sim 0$ is false and part of the input water is retained in the soil.

To assess whether the upper layer storage change can account for part of this discrepancy, the water balance over the entire observation period is corrected by including ΔS_{upper} as an approximation of the total storage change. For compartment B this gives ET = P - D - ΔS_{upper} = 350.6 − 51.8 - 45.4 = 253.4

mm. This is still higher than the reference value of 42.8 mm, indicating that the upper layer storage change alone cannot explain the discrepancy.
Two explanations are considered for the remaining difference. First, the upper layer storage change may not be representative of the storage change over the full soil profile, since the upper layer storage only considers the upper 0.35 m of the approximately 1.15 m deep soil profile. The actual storage increase over the full profile could therefore be larger than the 45.4 mm estimated from the upper layer alone, which would bring the corrected ET closer to the reference value.

Second, section 2.3.1 discusses the difference between the precipitation values from the Green Village weather station and the Rotterdam Airport station. The cumulative precipitation over the entire period (350.6 mm) is used in the water balance over the entire observation period that is described here. If instead the cumulative precipitation data of Rotterdam Airport (260.2 mm) is used, the water balance over the entire observation period for compartment B would become ET = 260.2 -51.8 = 208.4 mm, assuming that the net storage change is zero. When it is not assumed that the net storage change is zero and the upper layer storage change is considered as the storage change component, the water balance would become ET = 260.2 -51.8 - 45.4 = 163.0 mm. Although this is closer to the reference ET of 42.8 mm then when the dataset of the Green Village is used, the same uncertainties unaccounted storage change remain.
It is not possible to determine from the available data which of these explanations dominates, or to what extent both contribute to the observed discrepancy.

In summary, although compartment B shows plausible drainage values, a trustworthy water balance cannot be constructed for this compartment. The storage change term remains incompletely determined, and the gap between the reference ET (42.8 mm) and the rest term of the water balance is too large. It remains unclear whether this discrepancy stems from an overestimation of cumulative precipitation, false or incomplete assumptions about net storage change, or a combination of the two

4

Conclusions

This thesis investigated whether the minimal water demand of urban green spaces can be determined experimentally, by applying a mass balance approach to MeSUDa, an isolated vegetated bioswale located at the Flood Proof Holland site on the TU Delft campus. The observation period ran from 17 October 2025 to 19 January 2026. By measuring precipitation, outgoing drainage, and changes in water storage, evapotranspiration was to be determined as the rest term of the water balance. The following conclusions can be drawn.

The sensor data quality check showed that not all compartments could be used to apply the mass balance method. Compartments A and C had unreliable outgoing drainage measurements, attributed to tipping bucket malfunctioning and leakage through the LDPE lining or the seals around the outlet drainage pipes. As a result, only compartment B can be used to apply the mass balance method to.

For compartment B, the precipitation and outgoing drainage components could be determined. The cumulative precipitation over the entire observation period was 350.6 mm, though this value carries uncertainty due to a 34% discrepancy with precipitation data from the official KNMI station at Rotterdam The Hague Airport, which recorded 260.2 mm over the same period. The cumulative outgoing drainage of compartment B was 51.8 mm, which is below the reference bound established from the water balance and is therefore considered possible.

The storage change component could not be fully quantified for the entire soil profile. The upper layer storage estimation, based on soil moisture sensors at 10 and 25 cm depth, only represents the upper 0.35 m of the approximately 1.15 m deep soil profile. The nighttime water balance analysis showed that the upper layer storage change does not capture the full soil profile response, as a consistent offset was observed between the net input and the upper layer storage change. Attempts to quantify the lower bound of water storage on the vegetation and the first 10 cm of soil using an event-based rainfall threshold method and a graphical approach produced results that could not be reliably compared between the pre- and post-pruning periods, due to differences in antecedent soil moisture conditions and the number of qualifying rainfall events in each period. This did not lead to a reliable estimate for the lower bound storage capacity of the storage on the vegetation. The time lag analysis between the two soil moisture sensors using cross-correlation and dynamic time warping did not produce physically interpretable results that could be used to further constrain the storage change in the deeper parts of the soil profile.

Because the storage change component for the entire soil profile could not be determined, the cumulative water balance over the entire observation period could not be closed. Under the assumption that the net storage change over the entire period is zero, the rest term of the water balance gives a cumulative evapotranspiration of 298.8 mm for compartment B. This is far higher than the Makkink reference evapotranspiration of 42.8 mm for the same period, which indicates that this assumption is likely incorrect and that a substantial part of the precipitation is retained in the soil. When the upper layer storage change of 45.4 mm is included as an approximation of the total storage change, the corrected evapotranspiration is 253.4 mm, which is still far above the reference value. It was not determined whether

the remaining difference of the water balance ET relative to the Makkink reference value is primarily caused by an underestimation of the storage change over the full soil profile or an overestimation of input precipitation data by incorrect precipitation data or a combination of these factors.

In answer to the research question: ”Is it possible to determine the minimal water demand of urban green spaces experimentally?” the conclusion of this thesis is that, within the current setup and observation period, it was not possible. The mass balance approach applied to MeSUDa is in principle well suited to determine evapotranspiration as a proxy for the water demand of the vegetation. However, the reliable determination of all components of the water balance is a necessary condition for this approach to work. In this study, the outgoing drainage component could only be reliably determined for one out of three compartments, and the storage change component could not be fully quantified for the entire soil profile. As a result, water balance closure could not be achieved and a trustworthy estimate of the (cumulative) evapotranspiration, and therefore the water demand of the vegetation, could not be obtained.

5

Recommendations

5.1. Further verification of precipitation data

There are uncertainties regarding the reliability of the precipitation data used in this study, particularly when compared with data from the official KNMI weather station at Rotterdam Airport. It is therefore recommended to include precipitation data from a third weather station to allow for additional comparison. The proposed station is the weather station at the Zweth, which is located approximately 2 km from the FPH site. If the data from this station also differs substantially from the precipitation data used in this study, it is recommended to install a dedicated weather station near MeSUDa in order to obtain more site-specific precipitation measurements.

5.2. Outgoing drainage component validation

The outgoing drainage data obtained from the tipping buckets from compartment A and C did not behave as expected. It therefore should be tested if the tipping buckets are still functioning correctly and the possibility of another not registered outflow from the compartments should be investigated in order to close the water balance. To verify that the tipping buckets of the compartments can correctly measure outflow, a known quantity of water can be applied to the compartments. This known quantity of water can be ”irrigated” by the 60L water can (see table 2.4) close to the outlet of the compartment. In the days following this irrigation of the compartments, the tipping bucket data should be retrieved. When the tipping bucket of compartment A still does not register any values, the possibility of possible leakage should be investigated or the outlet drainage pipe should be checked for clogging. If these possibilities are ruled out, the most likely explanation will be that the tipping bucket malfunctions. It should then be removed from the MeSUDa set-up and checked if the water quantity to tip conversion is performed correctly. To rule out the possibility that the water standing in the drainage ditch below the tipping buckets is influencing the sensors, a permanent pump can be installed to prevent the water from entering the tipping buckets from below. Lastly because the divers did not detect any water level build up in compartment C indicating a leak. It should be investigated if the water is leaking through the plastic lining or the seal between the foundation wall and under drain. After the leak has been identified, it should be patched and the diver data should be checked for any water level build up inside the compartment

5.3. Quantifying storage change over the whole soil profile

In order to quantify storage change for the whole profile, more information is necessary to know what is happening below the upper layer of MeSUDa. A soil moisture sensor could be placed at the bottom of the fine sand layer, below the pair that is already placed in the upper layer. This will provide an additional information point about the soil moisture level. This information can be used to extend the existing the vertical soil moisture profile $\theta(z)$ of equation 2.3. Now $\theta(z)$ is linear, but the addition of this extra soil moisture sensor can make a profile that is of a higher dimension.

5.4. Change of observation period and observation length

The observation period of this project was from 17-10-25 until 19-01-26. During these months the evapotranspiration was considerably lower than the summer months. Because the main objective of the project was to estimate the evapotranspiration, an observation spanning the summer months would be more suitable. More specifically, targeting a dry period in the summer months could be more meaningful to answer the question of what is the minimal water demand of plants. Then, the plants are more water stressed than in the current observation period, where there was relatively high precipitation. In section 3.2.3, the results of the water balance over the entire observation period is presented under the assumption that net storage change over a sufficiently large period would be 0. Within the current observation period, it could not be determined if the net change is zero, given the uncertainties over storage change estimation and outgoing drainage values. It is recommended to observe for a longer period than the 94 days of this project after the uncertainties over storage change estimation and outgoing drainage values have been taken away.

References

[1] Sharmila Jagadisan. “Promoting integrated blue–green infrastructure for urban resilience—lessons learned from case studies”. In: *Frontiers in Water* Volume 6 - 2024 (2024). ISSN: 2624-9375. DOI: 10.3389/frwa.2024.1474411. URL: https://www.frontiersin.org/journals/water/articles/10.3389/frwa.2024.1474411.

[2] Francisco García Sánchez and Dhanapal Govindarajulu. “Integrating blue-green infrastructure in urban planning for climate adaptation: Lessons from Chennai and Kochi, India”. In: *Land Use Policy* 124 (2023), p. 106455. ISSN: 0264-8377. DOI: https://doi.org/10.1016/j.landusepol.2022.106455. URL: https://www.sciencedirect.com/science/article/pii/S0264837722004823.

[3] Zahra Ghofrani, Victor Sposito, and Robert Faggian. “A Comprehensive Review of Blue-Green Infrastructure Concepts”. In: *International Journal of Environment and Sustainability* 6.1 (2017), pp. 15–36. DOI: 10.24102/ijes.v6i1.728. URL: https://doi.org/10.24102/ijes.v6i1.728.

[4] United Nations Environment Programme. *Beating the Heat: A Sustainable Cooling Handbook for Cities*. UNEP, 2021. URL: https://wedocs.unep.org/handle/20.500.11822/37313.

[5] Tim D. Fletcher et al. “SUDS, LID, BMPs, WSUD and more – The evolution and application of terminology surrounding urban drainage”. In: *Urban Water Journal* 12.7 (2015), pp. 525–542. DOI: 10.1080/1573062X.2014.916314. eprint: https://doi.org/10.1080/1573062X.2014.916314. URL: https://doi.org/10.1080/1573062X.2014.916314.

[6] Joanna Boguniewicz-Zabłocka and Ewelina Łukasiewicz. “Blue–Green Infrastructure Effectiveness for Urban Stormwater Management: A Multi-Scale Residential Case Study”. In: *Land* 14.7 (2025). ISSN: 2073-445X. URL: https://www.mdpi.com/2073-445X/14/7/1340.

[7] Walelign Ayaliew Derseh et al. “Assessing the effectiveness of blue-green infrastructure for flood mitigation and alternative water supply provision: a watershed-scale study in Bahir Dar City, Ethiopia”. In: *Blue-Green Systems* 7.2 (Apr. 2025), pp. 261–286. ISSN: 2617-4782. DOI: 10.2166/bgs.2025.046. eprint: https://iwaponline.com/bgs/article-pdf/7/2/261/1585125/bgs2025046.pdf. URL: https://doi.org/10.2166/bgs.2025.046.

[8] Marc Breulmann, Roland Arno Müller, and Manfred van Afferden. “Modelling urban stormwater and irrigation management with coupled blue-green infrastructure in the context of climate change”. In: *Blue-Green Systems* 6.1 (Mar. 2024), pp. 100–113. ISSN: 2617-4782. DOI: 10.2166/bgs.2024.101. eprint: https://iwaponline.com/bgs/article-pdf/6/1/100/1398635/bgs0060100.pdf. URL: https://doi.org/10.2166/bgs.2024.101.

[9] Wen Zhou et al. “How can urban green spaces be planned to mitigate urban heat island effect under different climatic backgrounds? A threshold-based perspective”. In: *Science of The Total Environment* 890 (2023), p. 164422. ISSN: 0048-9697. DOI: https://doi.org/10.1016/j.scitotenv.2023.164422. URL: https://www.sciencedirect.com/science/article/pii/S0048969723030437.

[10] Ranhao Sun and Liding Chen. “Effects of green space dynamics on urban heat islands: Mitigation and diversification”. In: *Ecosystem Services* 23 (2017), pp. 38–46. ISSN: 2212-0416. DOI: https://doi.org/10.1016/j.ecoser.2016.11.011. URL: https://www.sciencedirect.com/science/article/pii/S2212041616301772.

[11] L. Gobatti, P.M. Bach, M. Maurer, et al. “Impact of soil moisture content on urban tree evaporative cooling and human thermal comfort”. In: *npj Urban Sustainability* 5 (2025), p. 26. DOI: 10.1038/s42949-025-00220-0. URL: https://doi.org/10.1038/s42949-025-00220-0.

[12] Puay Yok Tan et al. “A method to partition the relative effects of evaporative cooling and shading on air temperature within vegetation canopy”. In: *Journal of Urban Ecology* 4.1 (July 2018), juy012. ISSN: 2058-5543. DOI: 10.1093/jue/juy012. eprint: https://academic.oup.com/jue/article-pdf/4/1/juy012/25146909/juy012.pdf. URL: https://doi.org/10.1093/jue/juy012.

[13] S.E Gill et al. “Adapting Cities for climate Change: The role of the green infrastructure”. In: *Built Environment* 33.1 (Mar. 2007), pp. 115–133. DOI: 10.2148/benv.33.1.115. URL: https://doi.org/10.2148/benv.33.1.115.

[14] Karin van der Wiel et al. “KNMI’23 Climate Scenarios for the Netherlands: Storyline Scenarios of Regional Climate Change”. In: *Earth’s Future* 12.2 (2024). e2023EF003983 2023EF003983, e2023EF003983. DOI: https://doi.org/10.1029/2023EF003983. eprint: https://agupubs.onlinelibrary.wiley.com/doi/pdf/10.1029/2023EF003983. URL: https://agupubs.onlinelibrary.wiley.com/doi/abs/10.1029/2023EF003983.

[15] Hamideh Nouri, Sattar Chavoshi Borujeni, and Arjen Y. Hoekstra. “The blue water footprint of urban green spaces: An example for Adelaide, Australia”. In: *Landscape and Urban Planning* 190 (2019), p. 103613. ISSN: 0169-2046. DOI: https://doi.org/10.1016/j.landurbplan.2019.103613. URL: https://www.sciencedirect.com/science/article/pii/S0169204618304754.

[16] F. Van Gaalen et al. *Klimaatrisico’s in Nederland: de huidige stand van zaken*. Tech. rep. Den Haag, the Netherlands: PBL Planbureau voor de Leefomgeving, 2024. URL: https://www.pbl.nl/system/files/document/2024-05/pbl-2024-klimaatrisicos-in-nederland-5359.pdf.

[17] Sonia Reyes-Paecke et al. “Irrigation of green spaces and residential gardens in a Mediterranean metropolis: Gaps and opportunities for climate change adaptation”. In: *Landscape and Urban Planning* 182 (Nov. 2018). DOI: 10.1016/j.landurbplan.2018.10.006.

[18] Ekaterina Andrusenko et al. “Estimating the impact of blue-green infrastructure on household water demand”. In: *Water Science and Technology* 92.1 (June 2025), pp. 96–111. ISSN: 0273-1223. DOI: 10.2166/wst.2025.088. eprint: https://iwaponline.com/wst/article-pdf/92/1/96/1577934/wst2025088.pdf. URL: https://doi.org/10.2166/wst.2025.088.

[19] Xuanchang Zhang et al. “Green space water use and its impact on water resources in the capital region of China”. In: *Physics and Chemistry of the Earth, Parts A/B/C* 101 (2017). Physics and Economics of Ecosystem Services Flows, pp. 185–194. ISSN: 1474-7065. DOI: https://doi.org/10.1016/j.pce.2017.02.001. URL: https://www.sciencedirect.com/science/article/pii/S1474706516303187.

[20] Perrine Hamel et al. “Low-cost monitoring systems for urban water management: Lessons from the field”. In: *Water Research X* 22 (2024), p. 100212. DOI: 10.1016/j.wroa.2024.100212.

[21] Manuel Esperon-Rodriguez et al. “Global trends in urban forest irrigation: Environmental influences, challenges and opportunities for sustainable practices across 109 cities worldwide”. In: *Sustainable Cities and Society* 130 (2025), p. 106510. ISSN: 2210-6707. DOI: https://doi.org/10.1016/j.scs.2025.106510. URL: https://www.sciencedirect.com/science/article/pii/S2210670725003865.

[22] Richard G. Allen et al. *Crop Evapotranspiration: Guidelines for Computing Crop Water Requirements*. FAO Irrigation and Drainage Paper 56. Rome, Italy: Food and Agriculture Organization of the United Nations, 1998. URL: https://www.fao.org/3/X0490E/X0490E00.htm.

[23] Miriam Coenders. *Evaporation: The Invisible Water Drain – Introduction*. https://miriamcoenders.nl/evaporation/introduction/. Accessed: Tuesday 19th May, 2026. 2010.

[24] Hamideh Nouri et al. “Water requirements of urban landscape plants: A comparison of three factor-based approaches”. In: *Ecological Engineering* 57 (2013), pp. 276–284. ISSN: 0925-8574. DOI: https://doi.org/10.1016/j.ecoleng.2013.04.025. URL: https://www.sciencedirect.com/science/article/pii/S0925857413001432.

[25] Hamideh Nouri et al. “Comparing Three Approaches of Evapotranspiration Estimation in Mixed Urban Vegetation: Field-Based, Remote Sensing-Based and Observational-Based Methods”. In: *Remote Sensing* 8.6 (2016), p. 492. DOI: 10.3390/rs8060492. URL: https://doi.org/10.3390/rs8060492.

[26] Stenka Vulova et al. “Modeling urban evapotranspiration using remote sensing, flux footprints, and artificial intelligence”. In: *Science of The Total Environment* 786 (2021), p. 147293. ISSN: 0048-9697. DOI: https://doi.org/10.1016/j.scitotenv.2021.147293. URL: https://www.sciencedirect.com/science/article/pii/S0048969721023640.

[27] Chris Denich and Andrea Bradford. “Estimation of Evapotranspiration from Bioretention Areas Using Weighing Lysimeters”. In: *Journal of Hydrologic Engineering* 15.6 (Jan. 2010), pp. 522–530. DOI: 10.1061/(asce)he.1943-5584.0000134. URL: https://doi.org/10.1061/(asce)he.1943-5584.0000134.

[28] Won Jun Jo et al. “Estimation of Evapotranspiration and Water Requirements of Strawberry Plants in Greenhouses Using Environmental Data”. In: *Frontiers in Sustainable Food Systems* Volume 5 - 2021 (2021). ISSN: 2571-581X. DOI: 10.3389/fsufs.2021.684808. URL: https://www.frontiersin.org/journals/sustainable-food-systems/articles/10.3389/fsufs.2021.684808.

[29] C. E. Martin. “Development of an Open-Air Laboratory to Test Nitrate Removal in Bioswales”. MA thesis. Delft, The Netherlands: Delft University of Technology, May 2025.

[30] R.L. Cahill. “Design, Construction and Modeling of an Experimental Setup for the long term Eco-hydrological behavior of a Live Pole Drain”. MA thesis. Delft, The Netherlands: Delft University of Technology, Feb. 2024.

[31] The Green Village. *Climate City Campus*. Retrieved February 16, 2026. n.d. URL: https://www.thegreenvillage.org/project/climate-city-campus/.

[32] Inc. Decagon Devices. *Decagon’s 5TM Soil Moisture and Temperature sensor manual*. Tech. rep. Version Version: March 11, 2016 — 12:02:41. Retrieved February 16, 2026. Decagon Devices, Inc., 2016. URL: https://dorgean.com/Uploads/datasheet/5TM.pdf.

[33] Van Essen Instruments B.V. *TD-Diver submersible water level datalogger*. https://www.vanessen.com/products/data-loggers/td-diver/. Accessed: 17-02-2026. 2026.

[34] Paul Hiemstra and Raymond Sluiter. *Interpolation of Makkink Evaporation in the Netherlands*. Tech. rep. TR-327. De Bilt, The Netherlands: Royal Netherlands Meteorological Institute (KNMI), Dec. 2011. URL: https://cdn.knmi.nl/knmi/pdf/bibliotheek/knmipubTR/TR327.pdf.

[35] Royal Netherlands Meteorological Institute (KNMI). *Overzicht van de neerslag en verdamping in Nederland (MONV)*. Accessed: 2026-03-31. 2026. URL: https://www.knmi.nl/nederland-nu/klimatologie/gegevens/monv.

[36] Ruisdael Observatory. *Ruisdael Observatory Data Catalog*. Delft University of Technology. 2025-2026. URL: https://ruisdael.citg.tudelft.nl/parsivel/PAR008_GreenVillage/ (visited on 02/27/2026).

[37] Ruth E. Dunn et al. “Tipping-bucket rain gauges: a review of the undercatch phenomenon, and methods for its reduction and correction”. In: *Weather* 80.6 (2025), pp. 196–205. DOI: https://doi.org/10.1002/wea.7736. eprint: https://rmets.onlinelibrary.wiley.com/doi/pdf/10.1002/wea.7736. URL: https://rmets.onlinelibrary.wiley.com/doi/abs/10.1002/wea.7736.

[38] Decagon Devices. *ECRN-100 Rain Gauge User Manual*. Accessed: 2025-09-16. Decagon Devices. 2025. URL: https://metergroup.com/products/ecrn-100-rain-gauge/.

[39] Albrecht Jungk and Norbert Claassen. *Ion Diffusion in the Soil–Root System*. Ed. by Donald L. Sparks. Vol. 61. Advances in Agronomy. Academic Press, 1997, pp. 53–110. DOI: https://doi.org/10.1016/S0065-2113(08)60662-8. URL: https://www.sciencedirect.com/science/article/pii/S0065211308606628.

[40] GeeksforGeeks. *Cross-Correlation*. https://www.geeksforgeeks.org/data-science/cross-correlation/. Last updated: 14 May, 2025; accessed: Tuesday 19th May, 2026. 2025.

[41] Paul Bourke. *Cross Correlation*. https://paulbourke.net/miscellaneous/correlate/. Published: August 1996; accessed: Tuesday 19th May, 2026. 1996.

[42] George E. P. Box et al. *Time Series Analysis: Forecasting and Control*. 5th ed. John Wiley & Sons, 2016. URL: http://swbplus.bsz-bw.de/bsz433960558cov.htm.

[43] GeeksforGeeks. *Dynamic Time Warping (DTW) in Time Series*. https://www.geeksforgeeks.org/machine-learning/dynamic-time-warping-dtw-in-time-series/. Last updated: 1 May, 2025; accessed on Tuesday 19th May, 2026. 2025.

[44] H. Sakoe and S. Chiba. “Dynamic programming algorithm optimization for spoken word recognition”. In: *IEEE Transactions on Acoustics, Speech, and Signal Processing* 26.1 (1978), pp. 43–49. DOI: 10.1109/TASSP.1978.1163055.

[45] StackWild. *Dynamic Time Warping (DTW) Explained*. https://www.youtube.com/watch?v=C5joZ6Bwvmk. YouTube video, accessed 2026. 2022.

A

Figures

A.1. Figures and Images chapter

(a) Schematic side view of MeSUDa

(b) Schematic top view of MeSUDa

Figure A.1: Schematic side and top views of MeSUDa (dimensions in cm). The structures volume is 24.4 m³ [29]

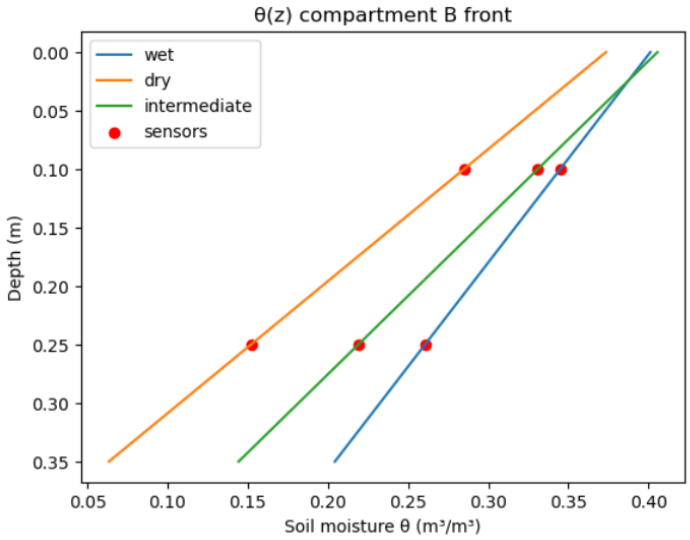

Figure A.2: Linear soil moisture profiles θ(z) for the first 0.35 m of upper soil, based on soil moisture measurements of three representative periods. This one is from compartment B.

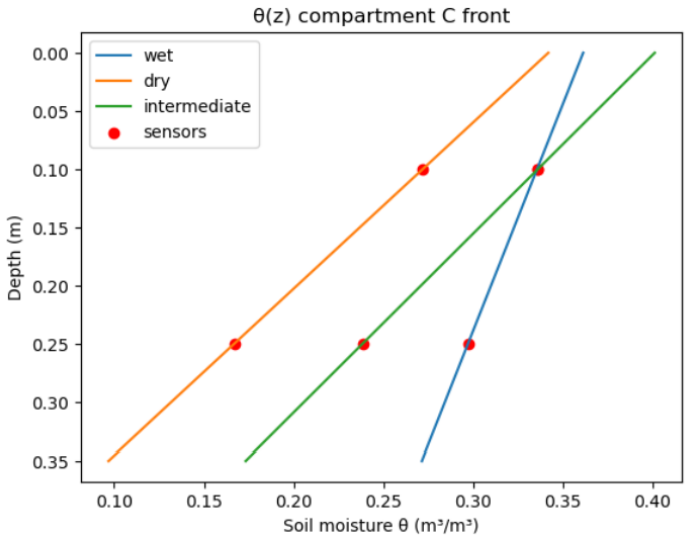

Figure A.3: Linear soil moisture profiles θ(z) for the first 0.35 m of upper soil, based on soil moisture measurements of three representative periods. This one is from compartment C.

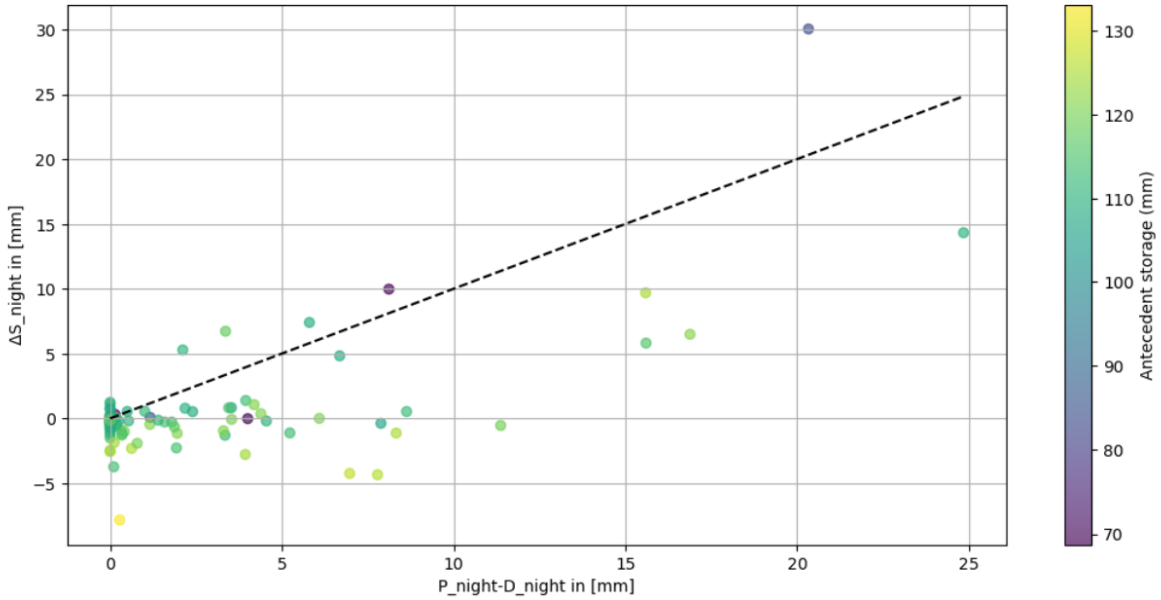

Figure A.4: Scatterplot of the net input in mm v.s. the change in upper layer storage over the night in mm of compartment A. The colored bar indicates the upper layer storage value at the beginning of each night

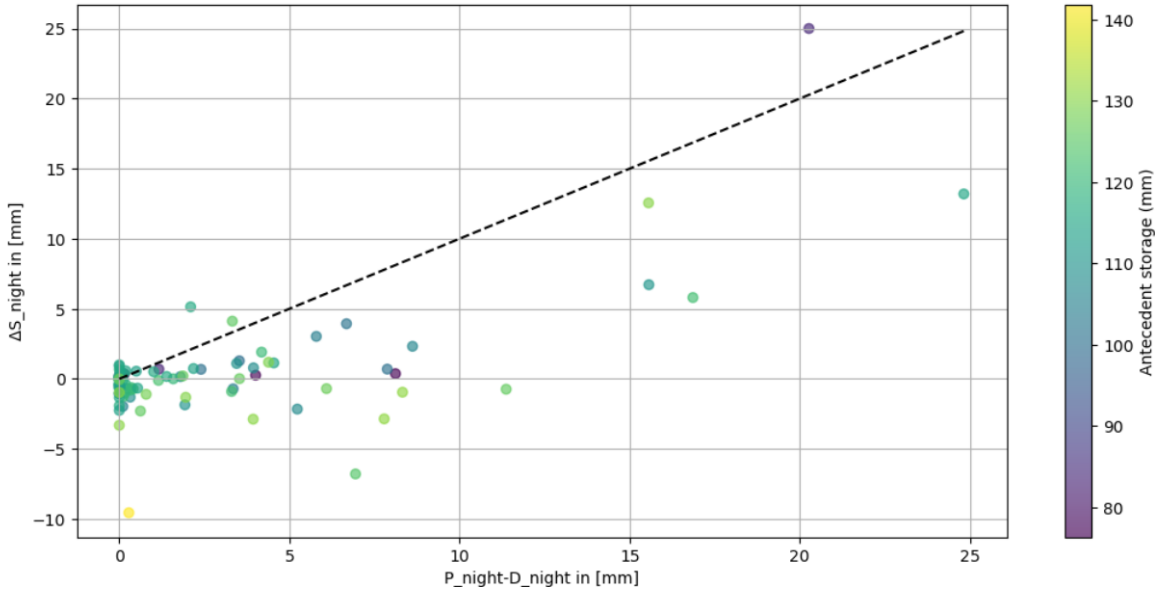

Figure A.5: Scatterplot of the net input in mm v.s. the change in upper layer storage over the night in mm of compartment C. The colored bar indicates the upper layer storage value at the beginning of each night

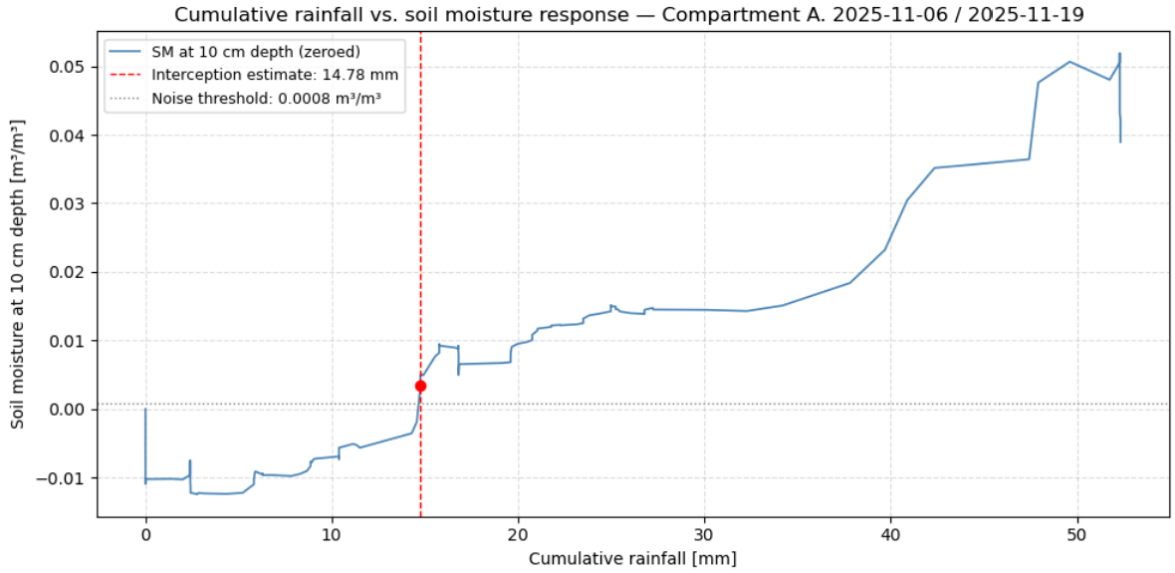

Figure A.6: Cumulative rainfall v.s. the zeroed soil moisture level at 10 cm depth in [mm] and [m³/m³] respectively. This is for compartment A in period 06-11-25 till 19-11-25

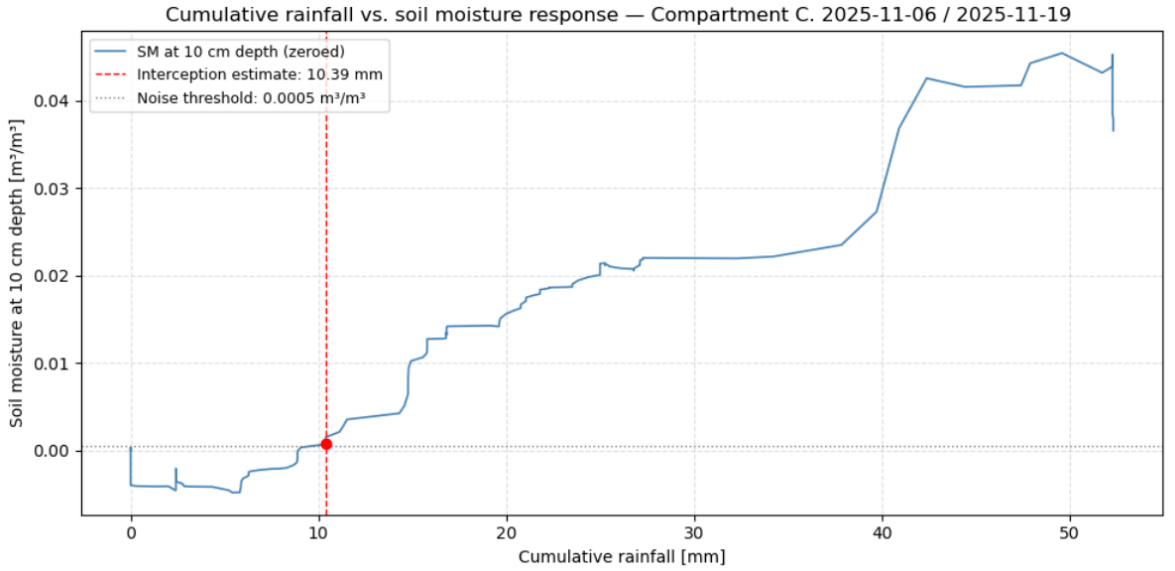

Figure A.7: Cumulative rainfall v.s. the zeroed soil moisture level at 10 cm depth in [mm] and [m³/m³] respectively. This is for compartment C in period 06-11-25 till 19-11-25